



**FREQUENCY DEPENDENCE OF TOTAL GATE
CAPACITANCE OF SUBMICRON INVERSION MOS
STRUCTURES**

by

623.815
1995
ZAH

Mohammad Zahangir Kabir

A Thesis

Submitted to the Department of Electrical and Electronic Engineering in partial
fulfilment of the requirements for the degree of

of

Master of Science in Electrical and Electronic Engineering.

DEPARTMENT OF ELECTRICAL AND ELECTRONIC ENGINEERING.
BANGLADESH UNIVERSITY OF ENGINEERING AND TECHNOLOGY.
DHAKA-1000, BANGLADESH.

JANUARY, 1995.




The thesis titled, "Frequency dependence of total gate capacitance of submicron inversion MOS structures", submitted by Mohammad Zahangir Kabir, Roll No.: 921324P, Registration No.: 87235 of M. Sc. in Engineering has been accepted as satisfactory in partial fulfilment of the requirements for the degree of

Master of Science in Electrical and Electronic Engineering.

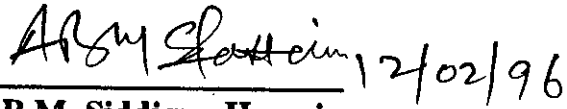
Board of Examiners:

1.


Dr. M.M. Shahidul Hassan
Professor
Department of Electrical and Electronic Engg.,
BUET, Dhaka-1000.


Chairman
(Supervisor)

2.


Dr. A.B.M. Siddique Hossain
Professor & Head
Department of Electrical and Electronic Engg.,
BUET, Dhaka-1000.

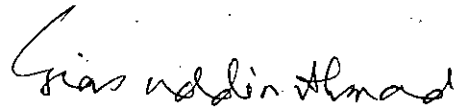
Member
(Ex-officio)

3.


Dr. Md. Rezwan Khan
Associate Professor
Department of Electrical and Electronic Engg.,
BUET, Dhaka-1000.

Member

4.


Dr. Gias Uddin Ahmad
Professor & Head
Department of Physics,
BUET, Dhaka-1000.


Member
(External)

DECLARATION


I hereby declare that this thesis work has been done by me and it has not been submitted elsewhere for the award of any degree or diploma .



Countersigned



(Dr. M.M. Shahidul Hassan)



(Mohammad Zahangir Kabir)

CONTENTS

Acknowledgment	iv
Abstract	v
List of Figures	vii

1. INTRODUCTION

1.1 Capacitance of MOS structures	1
1.2 Quantum effects on inversion layer capacitance	11
1.3 Frequency dependence of total gate capacitance	13
1.4 Review of recent works on MOS capacitance	15
1.5 Objective of this thesis	16
1.6 Summary of the dissertation	17

2. DETERMINATION OF SUBBAND ENERGIES

2.1 Introduction	18
2.2 Variational method	19
2.2.1 Principle of the method	20
2.2.2 Application to excited states	22
2.3 Mathematical expression for energy levels	23

2.3.1	Ground state	25
2.3.2	Excited energy states	31
2.4	Conclusions	33

3. ANALYSIS FOR FREQUENCY DEPENDENCE OF TOTAL GATE CAPACITANCE

3.1	Introduction	34
3.2	Charge concentration in three subbands	35
3.3	Surface potential and related equations considering quantum mechanical effects	36
3.4	Analytical expression for inversion layer quantum capacitance	40
3.5	Frequency dependence of total gate capacitance of inversion MOS structure	41
3.6	Conclusions	48

4. RESULTS AND DISCUSSIONS

4.1	Introduction	50
4.2	Subband energies	51
4.2.1	Comparison with self-consistent results	58
4.3	Inversion layer carrier concentration	61
4.3.1	Electron concentration in three subbands	65
4.3.2	Depletion layer carrier concentration	65

4.3.3	Average spatial extent of the inversion layer electrons from the surface	65
4.4	Inversion layer quantum capacitance	70
4.5	Total gate capacitance	76
4.6	conclusions	79
5.	CONCLUSIONS	
5.1	Conclusions	81
5.2	Suggestions for future work	82
	REFERENCES	83
APPENDIX I :	Resistance associated with the diffusion current of electrons from the bulk to the edge of the depletion region	86
APPENDIX II :	Effective resistance of depletion region to flow of minority and majority carriers	89
APPENDIX III :	Resistance associated with the generation and recombination within the depletion region	91

ACKNOWLEDGMENT

The author would like to express his sincere and heartiest gratitude to Dr. M.M. Shahidul Hassan, Professor of the Department of Electrical and Electronic Engineering, BUET, for his continued guidance, friendly supervision, encouragement, cooperation and valuable suggestions to complete this work.

The author wishes to express his heartiest thanks and regards to Dr. A.B.M. Siddique Hossain, Professor and Head of the Department of Electrical and Electronic Engineering, BUET, for support to complete this work.

Sincere thanks to all colleagues and friends for their cooperation. The author is grateful to his mother, brothers and sisters for their encouragement.

ABSTRACT

The metal-oxide-semiconductor (MOS) structures is the core structure in modern day microelectronics. Advancement of the fabrication technology, submicron structures are possible to fabricate. The combination of higher substrate doping level and thinner gate oxides increases the electric field at SiO₂-Si interface to a level such that the energy band bending at SiO₂-Si interface under inversion condition is very steep. Thus, a narrow potential well is formed near SiO₂-Si interface and the classical treatment of inversion layer carrier becomes less appropriate as the bulk energy band split into discrete subbands at the surface. The effects of quantization can be most accurately modeled by solving the Schrodinger's and Poisson's equations self-consistently. It is very time consuming and unsuitable for incorporation within larger programs, such as device simulators. Therefore, it is necessary to develop a simple model which includes the quantization effects and requires less computational time. WKB (Wentzel-Kramers-Brillouin) or Airy function approximation method can be applied for the calculation of subband energies in the inversion layer if the potential profile is considered linear. But if the total electron concentrations within the inversion layer is comparable to the total impurity charges within the depletion region, potential profile will no longer be linear. The variational approximation method can be applied for an arbitrary potential profile to find analytical expression for subband energies if the wave functions are assumed to have a predetermined form.

In this thesis, the analytical expressions for first three consecutive subband energies are obtained by variational approximation method and the results are compared with those of the self-consistent results. It is found that the results of the variational approximation method agree well with that of the self-consistent results. In this work, the analytical expression of inversion layer capacitance is derived considering quantization effects and the Fermi-Dirac statistical distribution law. The analytical expression of total gate capacitance is obtained incorporating the thermally generated electrons within the depletion region and the flow of electrons from the bulk to the SiO₂-Si interface in the quantum capacitance calculated from energy subbands. It is found that the total gate capacitance of MOS structure depends on gate voltage and frequency. This work shows that the total gate capacitance decreases at high frequencies and increases at low frequencies. This work also compares the inversion layer quantum capacitance and the total gate capacitance with that of the classical calculations. Quantum mechanically calculated results are smaller than that of the classical results.

LIST OF FIGURES

1.1	The metal oxide-semiconductor structures	2
1.2	Energy band diagram of a p-type substrate MOS capacitor	4
1.3	Energy band diagram of p-type substrate at higher gate voltage	6
1.4	Energy band diagram of p-type substrate at the onset of strong inversion	8
1.5	Quantum effects on inversion layer	12
1.6	Low frequency (LF), high frequency (HF), and deep-depletion (DD) capacitance-voltage characteristics	14
3.1	Schematic band bending due to depletion and inversion layer charges	38
3.2	Equivalent circuit for p-type MOS capacitor in depletion-inversion mode after Lehovec and Slobodsky	42
3.3	Simplified equivalent circuit for p-type MOS capacitor with heavy inversion layer	45
4.1	Effect of surface electric field on the subband energy levels	52
4.2	Effect of surface potential on the subband energy levels	53
4.3	Effect of gate voltage on the subband energy levels	54
4.4	Effect of inversion layer charge on the subband energy levels	55
4.5	Subband energy levels vs. surface electric field for three different channel doping	56
4.6	Subband energy levels vs. gate voltage for three different channel doping	57

4.7	Subband energy levels vs. gate voltage characteristics calculated self-consistently	59
4.8	Inversion layer carrier concentration vs. surface potential	62
4.9	Inversion layer carrier concentration vs. gate voltage	63
4.10	Inversion layer carrier concentration vs. gate voltage for three different channel doping	64
4.11	Electron concentration in the three subbands vs. surface potential	66
4.12	Depletion carrier concentration vs. surface potential	67
4.13	Effect of inversion layer charge on average spatial extent of the inversion charges from the SiO_2 -Si interface	68
4.14	Effect of surface potential on average spatial extent of the inversion charges from the SiO_2 -Si interface	69
4.15	Inversion layer quantum capacitance vs. surface potential	71
4.16	Inversion layer quantum capacitance vs. gate voltage	72
4.17	Comparison of the effect of surface potential on inversion layer capacitance between classical and quantum mechanical calculations	73
4.18	Comparison of the effect of gate voltage on inversion layer capacitance between classical and quantum mechanical calculations	74
4.19	Inversion layer quantum capacitance vs. gate voltage for three different channel doping	75
4.20	Comparison of the effect of gate voltage on total gate capacitance between classical and quantum mechanical calculations	77

4.21 High frequency and low frequency capacitance-voltage characteristics for three different channel doping

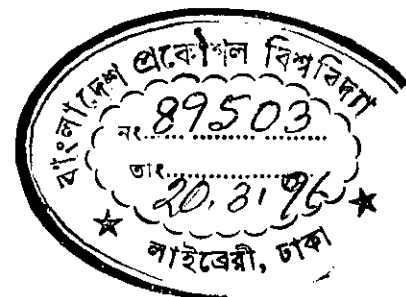
78

LIST OF TABLES

TABLE I : Parameters used for computational works.	51
TABLE II : Comparison of variational (var) and self-consistent (sc) values of energy E_{10} , E_{20} and E_{11} as a function of gate voltage for channel doping of $N_A = 1.1 \times 10^{24} \text{ m}^{-3}$.	60

CHAPTER 1

INTRODUCTION



1.1 Capacitance of MOS structures

Metal-oxide semiconductor (MOS) devices dominate the integrated circuit industry, both in numbers produced and in the variety of their applications. The two terminal MOS structure is the simplest of MOS devices and the structural heart of all MOS devices. Capacitance is of course the primary electrical observable exhibited by an MOS structure. The total gate capacitance of MOS structure depends on bias voltage and frequency. To the device specialist, the capacitance-voltage (C-V) characteristic is like a picture-window, a window revealing the internal nature of the structure. The characteristic serves as a powerful diagnostic tool for identifying deviations from the ideal in both oxide and the semiconductor. C-V characteristics are routinely monitored during MOS device fabrication.

The submicron MOS structure is a simple two terminal device composed of a thin (4 nm to 14 nm) SiO_2 layer sandwiched between a silicon substrate and a metallic field plate called gate (Fig. 1.1). The most common field plate materials are aluminum and heavily doped polycrystalline silicon. A second metallic layer present along the back or bottom side of the semiconductor provides an electrical contact to the silicon substrate. It is normally grounded and is called the substrate contact.

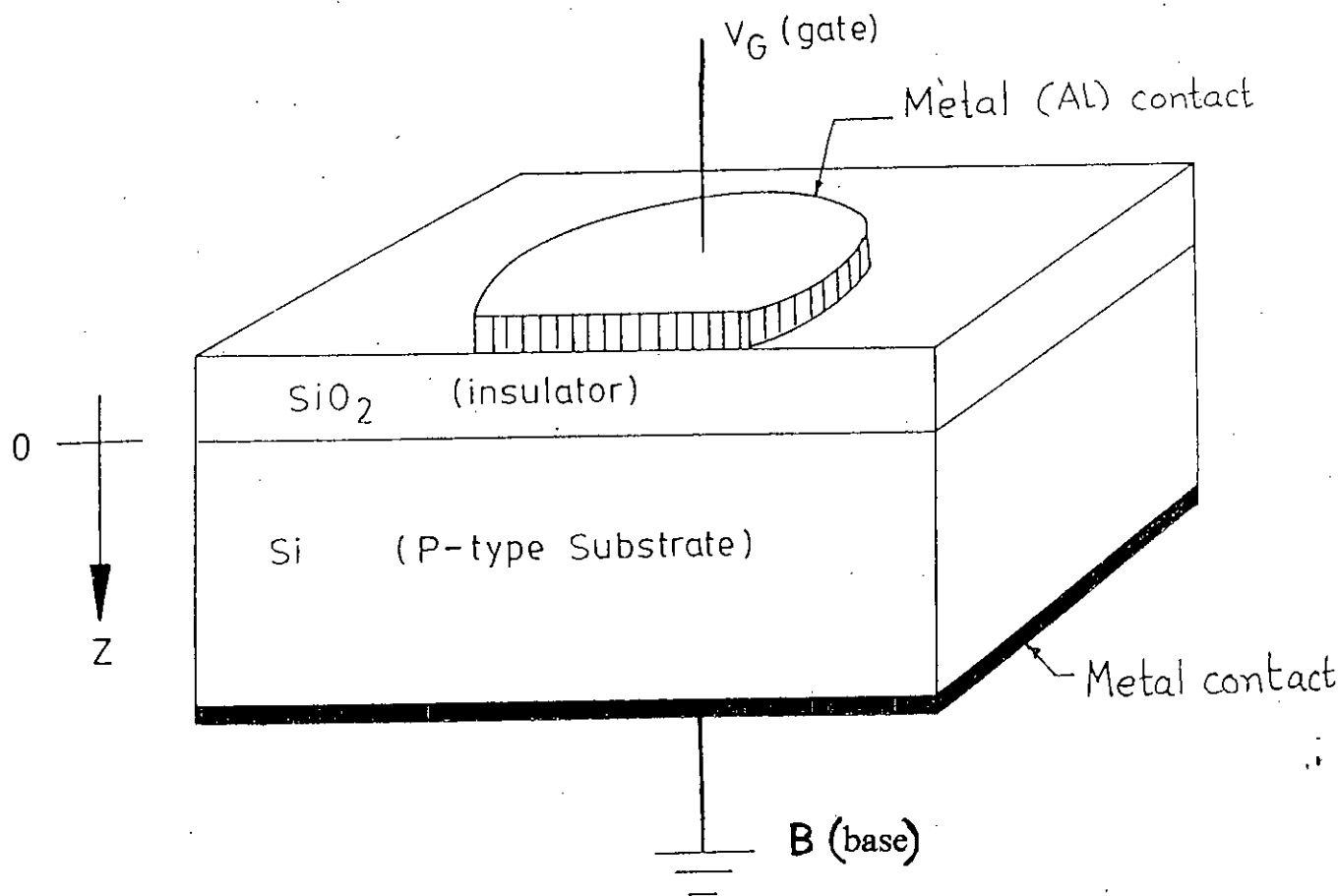


Fig. 1.1 The metal oxide-semiconductor structures

The ideal MOS structure has the following explicit properties:

- (i) The metallic gate is sufficiently thick so that it can be considered as equipotential region under ac as well as dc biasing conditions.
- (ii) The oxide is perfect insulator with zero current flowing through the layer under all static biasing conditions.
- (iii) There are no charge centers located in the oxide or at the oxide-semiconductor interface.
- (iv) The semiconductor is uniformly doped.
- (v) The semiconductor is sufficiently thick so that regardless of the applied gate potential, a field-free region (the so-called Si bulk) is encountered before reaching the back contact.

Electron and hole concentration in the silicon at equilibrium can be expressed as [1]:

$$n = n_i e^{\frac{q}{kT}(\psi - \phi_F)} \quad (1.1)$$

and

$$p = n_i e^{\frac{q}{kT}(\phi_F - \psi)} \quad (1.2)$$

Where, n_i is the intrinsic carrier concentration, k is Boltzmann's constant, T is the absolute temperature, ψ is the potential of the intrinsic energy level and ϕ_F is the Fermi potential (Fig 1.2). The potential ψ is assumed to be zero in the bulk. ψ evaluated at the oxide-semiconductor interface (at $z = 0$) is given the special symbol ψ_s and is known as the surface potential. The electron concentration can be written as

$$n = N_A e^{\frac{q}{kT}(\psi - 2\phi_F)} \quad (1.3)$$

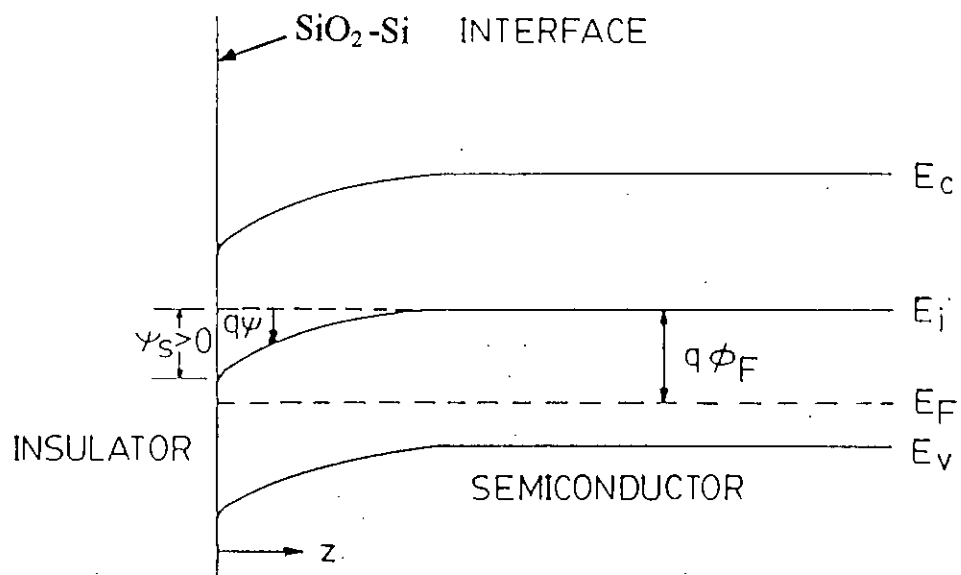


Fig. 1.2 Energy band diagram of a p-type substrate MOS structures

Where N_A is the doping density of the p-type substrate.

Positive gate voltage produce an electric field which bends the energy bands downward. For small positive gate voltage (Fig 1.3a) the holes will be repelled from the vicinity of the oxide-silicon interface leaving behind a space charge region of uncompensated ionized acceptor ions. Since in this region the concentration of carriers is negligible in comparison to the impurity concentration, it will be referred to as a depletion region. Upon further increase of gate voltage (Fig 1.3b), the bands at the semiconductor surface bend down more strongly which causes E_i below E_F and an inversion layer is formed. In that case, electrons (the minority carriers) will be attracted to the interface so that while some of the charge in the semiconductor will still consist of the charge of ionized acceptors, another part will consist of the electrons in the inversion layer. We consider that these electrons come from the relatively slow process of electron hole generation in the depletion region. This inversion layer near the semiconductor surface has conduction properties typical of n-type material.

The electron concentration at the surface is given by

$$n_{\text{surface}} = N_A e^{\frac{q}{kT}(\psi_s - 2\phi_F)} \quad (1.4)$$

At $\psi_s = \phi_F$, $n_{\text{surface}} = n_i$; intrinsic concentration as seen from equation (1.1) and from $np = n_i^2$; then $n_{\text{surface}} = p_{\text{surface}} = n_i$ this is defined as the limited point between the depletion and inversion regions. With increasing ψ_s above ϕ_F , n_{surface} increases drastically, and at $\psi_s = 2\phi_F$, we have $n_{\text{surface}} = N_A$.

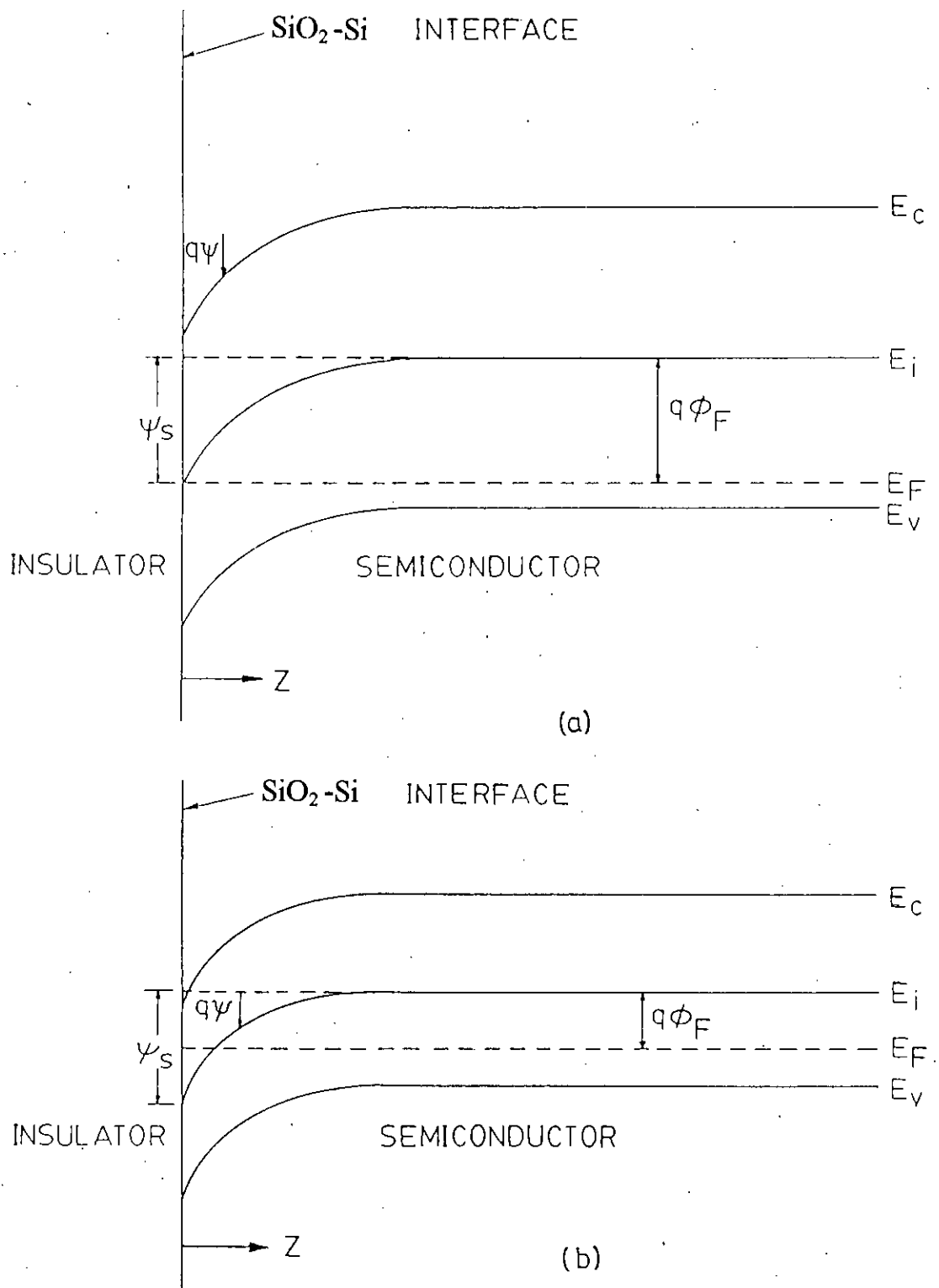


Fig. 1.3 Energy band diagram of p-type substrate at higher gate voltage

(a) Depletion (b) Inversion

This is known as the condition of the onset of strong inversion and this situation is shown in (Fig 1.4).

The density of induced charge in the semiconductor denoted by Q_s is given by Gauss' law ,

$$-Q_s = \epsilon_{ox} F_{ox} = \epsilon_s F_s \quad (1.5)$$

Where,

ϵ_{ox} = Permittivity of oxide

ϵ_s = Permittivity of semiconductor

F_{ox} = Electric field in the semiconductor

F_s = Electric field at the semiconductor surface

When the semiconductor surface is depleted the total ionized acceptors in the depletion region is given by

$$Q_B = -q N_A Z_d \quad (1.6)$$

Where, Z_d is the width of the depletion region. The relationship between ψ_s and Z_d can be obtained by solving Poisson's equation using the depletion approximation. The results is,

$$Z_d = \sqrt{\frac{2\epsilon_s \psi_s}{qN_A}} \quad (1.7)$$

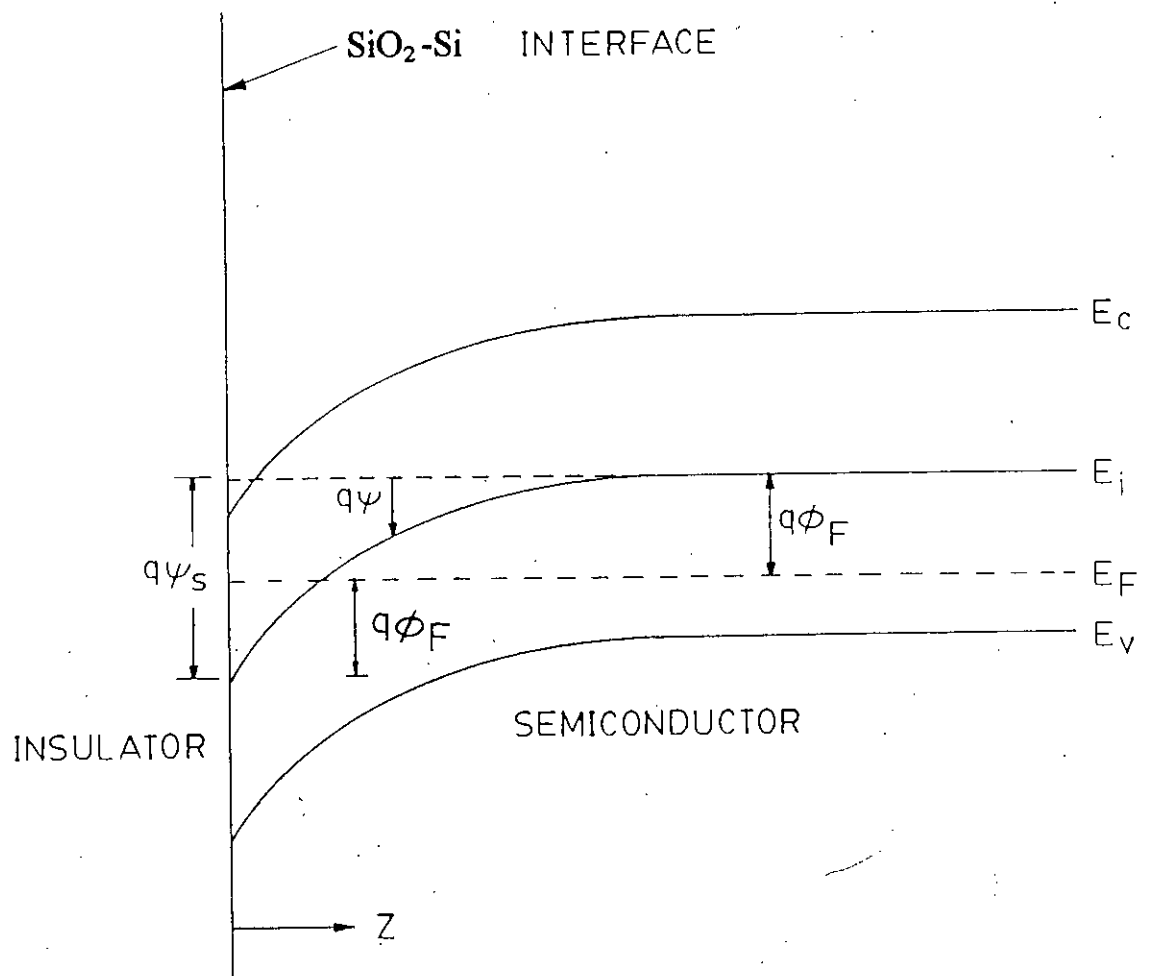


Fig. 1.4 Energy band diagram of p-type substrate at the onset of strong inversion

Once the strong inversion occurs, the depletion-layer width reaches a maximum. The depletion width is given by [2],

$$Z_{dm} \cong \sqrt{\frac{2\epsilon_s(2\phi_F)}{qN_A}} \quad (1.8)$$

Where,
$$\phi_F = \frac{kT}{q} \ln \frac{N_A}{n_i} \quad (1.9)$$

The electric field at the interface is given by [3],

$$F_s = \pm \frac{F\sqrt{N_A}}{\epsilon_s} \sqrt{\left\{ \left(\phi_t e^{\frac{-\psi_s}{\phi_t}} + \psi_s - \phi_t \right) + e^{\frac{-2\phi_F}{\phi_t}} \left(\phi_t e^{\frac{\psi_s}{\phi_t}} - \psi_s - \phi_t \right) \right\}} \quad (1.10)$$

Where, $F = \sqrt{2q\epsilon_s}$ and the '+' sign for F_s is to be used with $\psi_s > 0$, and the '-' sign with $\psi_s < 0$; $\phi_t = \frac{kT}{q}$, and the total semiconductor charge per unit area Q_s , is given as :

$$Q_s = \pm F\sqrt{N_A} \sqrt{\left\{ \left(\phi_t e^{\frac{-\psi_s}{\phi_t}} + \psi_s - \phi_t \right) + e^{\frac{-2\phi_F}{\phi_t}} \left(\phi_t e^{\frac{\psi_s}{\phi_t}} - \psi_s - \phi_t \right) \right\}} \quad (1.11)$$

The total charge Q_s (per unit area) below the oxide is the sum of the charge due to the electrons in the inversion layer Q_{inv} and the charge due to the ionized acceptor atoms in the depletion region Q_B ,

$$Q_s = Q_{inv} + Q_B \quad (1.12)$$

The small signal capacitance per unit area corresponding to the semiconductor charge regions denoted by

$$C_s = -\frac{dQ_s}{d\psi_s} \quad (1.13)$$

From equation (1.12)

$$C_s = -\frac{dQ_{inv}}{d\psi_s} - \frac{dQ_B}{d\psi_s} \quad (1.14)$$

We have then separated the total semiconductor capacitance C_s into two components, one owing to the depletion region charge and one owing to the inversion layer charge. So, we can define a inversion region incremental capacitance per unit area [3],

$$C_I = -\frac{dQ_{inv}}{d\psi_s}$$

$$C_I = F\sqrt{N_A} \frac{e^{\frac{(\psi_s - 2\phi_F)}{\phi_t}}}{2\sqrt{\psi_s + \phi_t e^{\frac{(\psi_s - 2\phi_F)}{\phi_t}}}} \quad (1.15)$$

We can also define a depletion region incremental capacitance per unit area[4],

$$C_D = -\frac{dQ_B}{d\psi_s}$$

$$= \left(\frac{q\epsilon_s N_A}{2\psi_s} \right)^{\frac{1}{2}} = \frac{\epsilon_s}{Z_d}$$

$$C_D = \frac{\epsilon_s}{Z_d} \quad (1.16)$$

1.2 Quantum effects on inversion layer capacitance

The need for careful treatment of inversion layer quantization has recently become more pressing due to the increasing impact of the quantization on submicron MOS structures with the reduced gate oxide thickness and increased channel doping required in scaled devices. The combination of higher doping levels and thinner gate oxides increases the electric field at the SiO_2 -Si interface to a level such that the energy-band bending at the SiO_2 -Si interface under inversion condition is very steep. So, a potential well is created. The confinement of the carriers in this potential well leads to a two-dimensional electron gas (2DEG) system. Therefore in order to accurately simulate the inversion carriers in submicron MOS devices, models that incorporate the two-dimensional quantum nature of the carriers are necessary.

The quantum mechanical picture differs in several aspects from the classical one [5]. The bulk conduction energy band is split into discrete subbands in the inversion layer, with the lowest subband shifted substantially above the conduction band minimum (Fig 1.5). Hence a larger surface potential is needed for a given channel charge. This has the effect of decreasing the inversion layer charge density for a given gate voltage. In addition, because of the quantum mechanical nature of 2DEG, the distribution of carriers is displaced away from the Si-SiO₂ interface and the average distance of the spatial distribution of the inversion layer charge from the interface is larger. Hence, a larger band bending is needed for a given population in the conduction band.

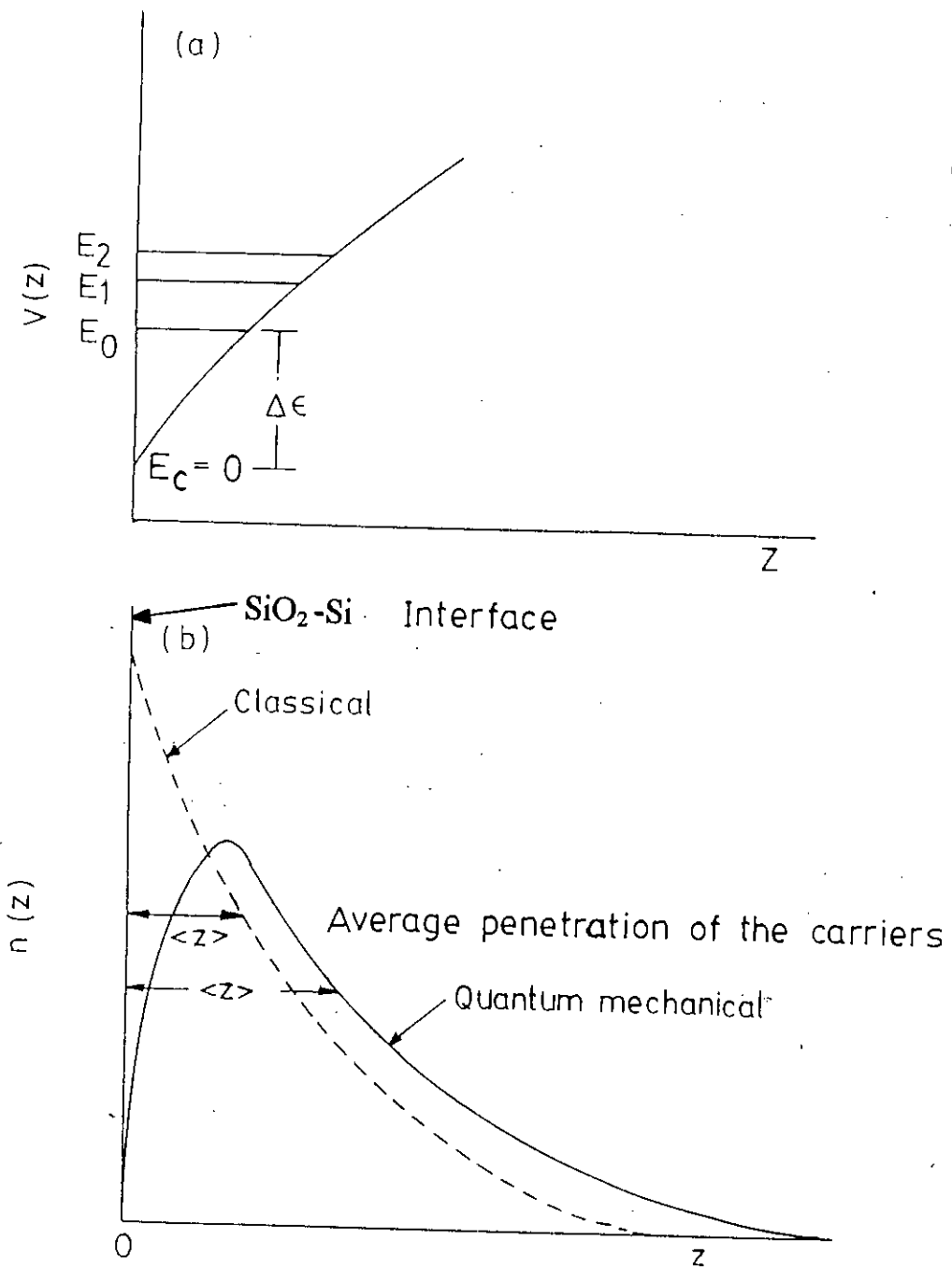


Fig. 1.5 Quantum effects on inversion layer

(a) Discretisation of energy levels

(b) Spatial distribution of charge carriers

Considering all the effects we conclude that the inversion layer capacitance(C_I) is decreased when compared to the classical value.

1.3 Frequency dependence of total gate capacitance

The capacitance of a semiconductor device, with its non-linear charge-voltage relationship, is defined by [4]

$$C = \frac{dQ}{dV} \quad (1.17)$$

Viewed from the gate, the MOS capacitance becomes ,

$$C_G = \frac{dQ_G}{dV_G} \quad (1.18)$$

The expression of C_G , can be written as ,

$$C_G = \frac{1}{\frac{1}{C_0} + \frac{1}{C_D + C_I}} \quad (1.19)$$

Where, C_0 is the oxide capacitance, C_D and C_I are the depletion and inversion layer capacitances respectively.

The complete description of frequency dependence of MOS structures is shown in Fig. 1.6. When the devices is driven from accumulation into depletion, the inversion layer charge is negligible compared with the depletion layer charge. As a result $C_I = 0$. So, C_G is merely C_0 in series with C_D . As the gate voltage continues to increase, the surface becomes strongly inverted if

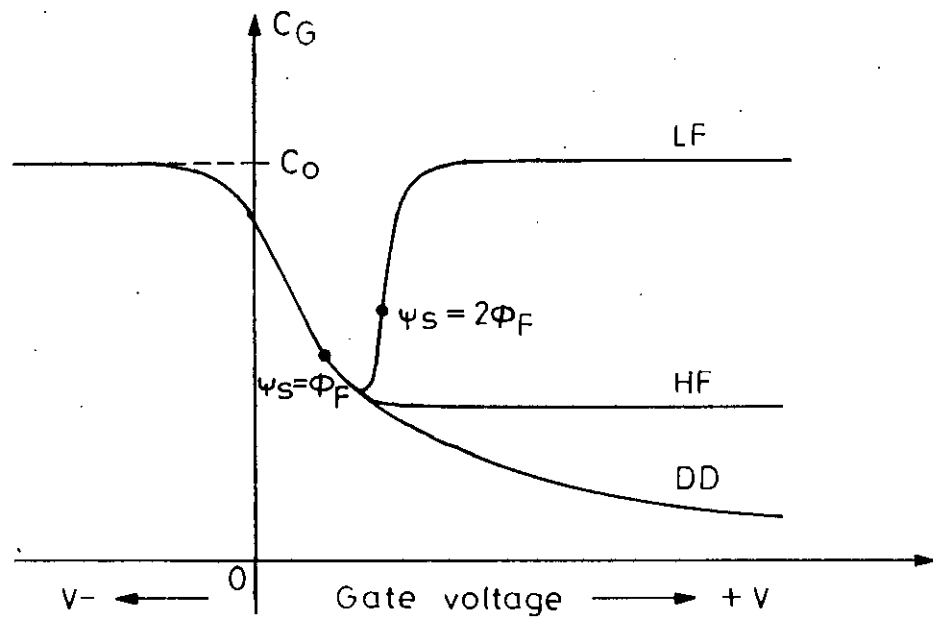


Fig. 1.6 Low frequency (LF), high frequency (HF), and deep-depletion (DD) capacitance-voltage characteristics [Ref. 4].

the gate voltage is swept slowly enough to allow generation of minority carriers required for formation of this inversion layer. If the ac probing voltage used in the capacitance measurement is of sufficiently low frequency that the inversion charge is able to follow the ac probing voltage and the dc sweeping voltage, then the low frequency (LF) curve is obtained. If the ac voltage frequency is too high, but the dc sweep voltage rate is sufficiently low, then the high frequency (HF) curve is measured. If the sweep voltage rate is too high and there is not enough time for the inversion charge to be thermally generated, then the deep depletion (DD) curve is obtained regardless of the frequency of the ac probing voltage.

1.4 Review of recent works on MOS capacitance

The Two-dimensional quantum nature of the electrons in inversion layers has been studied in details by a number of researches [5,6] by solving Schrodinger's and Poisson's equation self-consistently. In these work, the electron inversion layer charge density is obtained self-consistently utilizing Schrodinger's and Poisson's equations. C. Moglestue[5] also compared the self-consistent and Airy function (Solution of Schrodinger's equation for a triangular potential well) normalized charge density for inversion electrons in the SiO₂-Si system. Recently simple and approximate models have also been proposed [7,8] and their implementation in classical device simulators described. In these works, the authors proposed a modified semi-quantum mechanical method for the calculation of inversion layer carrier concentration and compared the modified calculations with that of the self-consistent quantum mechanical calculations.

Two-dimensional (2DEG) electron gas in a quantum well or inversion layer, unlike an ordinary grounded metallic plate, does not completely screen an applied electric field. A 2DEG manifests itself as a capacitance in series in the direction transverse to the quantum well [9]. Recent analytical works [10,11] have carried out for determination of energy subbands and capacitance in the inversion layer. to find the dependence of frequency on capacitance, the thermally generated electrons within the depletion region and the flow of electrons from the bulk to the Si-SiO₂ interface need to be incorporated in the quantum capacitance calculated from energy subbands. Recent works on this issues have been carried out on Double-barrier tunneling structure [12] but not on MOS structures.

1.5 Objective of this thesis

The main objective of this research is to obtain an analytical expression of total gate capacitance of an inversion MOS structure as a function of gate voltage and frequency. Inversion layer capacitance has significant contribution to the total gate capacitance. It is well known that the electrons of MOS inversion layer form subbands, each of which corresponds to a quantized level for motion in the direction perpendicular to the silicon-insulator surface. In this work, the analytical expressions of inversion layer capacitance is derived considering quantization effects and the Fermi-Dirac statistical distribution law. The expression for eigen energies of subbands is derived by applying the variational approximation method. To derive the analytical expression of total gate capacitance, the thermally generated electrons within the depletion region and the flow of electrons from the bulk to the SiO₂-Si interface is incorporated in

the quantum capacitance calculated from energy subbands. This work also compares the inversion layer quantum capacitance and the total gate capacitance with that of the classical calculations.

1.6 Summary of the dissertation

In this thesis work, the analytical expressions for inversion layer quantum capacitance and the total gate capacitance of MOS structure are derived in chapter three. The analytical expression of first three subband energies in the inversion layer are also derived in chapter two by using variational approximation method. The variational approximation method is described in chapter two.

Based on the analytical model developed in chapter two and three, the behavior of total gate capacitance is studied in chapter four. The results of quantum effects on inversion capacitance, inversion layer charge concentration, the electron concentration in the first three consecutive subbands and also the predicted difference between classically and quantum mechanically calculated inversion layer capacitances are studied in chapter four. Chapter five contains the concluding remarks along with suggestions for future work on this topics.

CHAPTER 2

DETERMINATION OF SUBBAND ENERGIES

2.1 Introduction

In MOS devices quantum effects play an important role even at room temperature, where the width of the inversion layer is of the same order of magnitude as the De Broglie wavelength of the electrons in the inversion layer. Therefore it becomes necessary to solve Schrodinger's equation for the subband energies and wave functions in order to study the transport properties of inversion layer electrons. In this case, since the potential energy term is connected to the electron density and thus to the wave functions through Poisson's equation, the determination of the subband structure requires the simultaneous and self-consistent solution of Schrodinger's and Poisson's equations.

However, the nonlinear coupling of these two equations prevents an analytical solution from being found, forcing one to make use of iterative numerical procedures. Although they are very accurate, they fail to provide information about the analytical character of wave functions at nonzero temperatures[13]. Moreover, fully numerical calculations require considerable computational effort, thus making them unsuitable for incorporation within larger programs, such as device simulators. So, several simpler methods are

developed that approximate the quantum mechanical calculation results and require the same CPU time as that of the classical calculation.

When only one subband is occupied, i.e., in the electric quantum limit, WKB (Wentzel-Kramers-Brillouin) can be used to find an analytical expression for the energy subbands. When more than one subband is occupied, Airy function approximation method can be used to find an analytical expression for the energy subbands. In both methods mentioned above, the potential profile within the inversion layer is considered linear. But if the total electron concentrations within the inversion layer is comparable to the total impurity charges within the depletion region, potential profile will no longer be linear. The variational method can be applied for an arbitrary potential profile to find analytical expression for energy subbands if the wave functions are assumed to have a predetermined form [6,14]. In this chapter variational method is used to find an analytical expression for energy subbands.

2.2 Variational method

The variation method can be used for the approximate determination of the energy levels of a system when there is no closely related problem that is capable of exact solution, so that the perturbation method is inapplicable. It can also be applied to the systems that are described by a nonseparable Schrodinger equation, in which case numerical solutions are extremely arduous and the WKB method cannot be used. The variational method is specially applicable for the determination of lowest energy state. In special cases variational method can be extended to the state of the system other than the lowest one.

2.2.1 Principle of the method

Let us consider an arbitrary physical system whose Hamiltonian H is time-independent. To simplify the notation, we shall assume that the entire spectrum of H is Discrete and non-degenerative [15],

$$H\phi_n = E_n \phi_n \quad ; \quad n = 0, 1, 2, \dots \quad (2.1)$$

Although the Hamiltonian H is known, this is not necessarily the case for its eigen values E_n and the corresponding eigen states ϕ_n .

Let us choose an arbitrary wave function ψ of the state space of the system. The mean value of Hamiltonian H in the state ψ is such that

$$\langle H \rangle = \frac{\langle \psi | H | \psi \rangle}{\langle \psi | \psi \rangle} \geq E_0 \quad (2.2)$$

(Where E_0 is the smallest eigen value of H), equality occurring if and only if ψ is an eigenvector of H with the eigenvalue E_0 .

To prove inequality (2.1), we expand the wave function ψ on the basis of eigenstates of H :

$$\psi = \sum_n C_n \phi_n \quad (2.3)$$

We then have

$$\langle \psi | H | \psi \rangle = \sum_n |C_n|^2 E_n \geq E_0 \sum_n |C_n|^2 \quad (2.4)$$

With $\langle \psi | \psi \rangle = \sum_n |C_n|^2 \quad (2.5)$

Which proves (2.2). For inequality (2.4) to become an equality, it is necessary and sufficient that all the coefficients C_n be zero, with the exception of C_0 ; ψ is then an eigenvector of H with the eigen value E_0 .

This property is the basis for a method of approximate determination of E_0 . We choose (in theory, arbitrarily, but in fact, by using physical criteria) a family of wave functions $\psi(\alpha)$ which depend on a certain number of parameters which we symbolize by α . We can calculate the mean value $\langle H \rangle(\alpha)$ of the Hamiltonian H in these states, and we minimize $\langle H \rangle(\alpha)$ with respect to the parameter α . The minimal value so obtained constitutes an approximation of the ground state E_0 of the system. The wave functions $\psi(\alpha)$ are called trail functions, and the method itself, the variational method.

2.2.2 Application to excited states

The variational method can also be used to obtain an upper limit for one of the higher energy levels if the trial function is orthogonal to the eigenfunctions of all the lower states [15]. Suppose that the energy levels are arranged in an ascending series ; E_0 , E_1 , E_2 Then if ψ is orthogonal to φ_j ; for $j = 0,1,2$ n ; it is easily seen from (2.3) that the corresponding expansion coefficients C_j are all zero . An inequality can be derived from (2.4) by replacing each eigen value E in the summation on the right by E_{n+1} . With the result that the expectation value of the energy is an upper limit on this eigen value .

The technique of choosing the trial function for evaluation of energy for any excited state is that this function must be orthogonal to the eigen functions of all the lower states (arranged in ascending order of energy). For example, if we want to calculate (approximately, in theory) the first excited state E_1 , we should choose trial function which are orthogonal to wave function of the ground state. This follows from the above discussion which shows that $\langle H \rangle$ has a lower bound of E_1 , and no longer of E_0 , if the coefficient C_0 is zero. Thus, the first excited state E_1 is determined. In this way we can determine the higher excited states.

2.3 Mathematical expression for energy levels

In formulating Schrodinger's equation for the two-dimensional electron gas (2DEG) system of the inversion layer of an N-channel MOS devices, it is assumed that the wave functions can be expanded in terms of Bloch waves traveling parallel to the interface constrained by an envelope function $\xi_{ij}(z)$ (for the j th subband in the i th valley) normal to the interface (i.e. in the z -direction). The envelope function is found to satisfy Schrodinger's equation [11]

$$\frac{\hbar^2}{2m_{zi}} \frac{d^2}{dz^2} \xi_{ij}(z) + [E_{ij} - V(z)] \xi_{ij}(z) = 0 \quad (2.6)$$

Where m_{zi} is the effective mass normal to the interface, $V(z)$ is the electrostatic potential, and E_{ij} is the eigen value of the j th subband in the i th valley. This equation must be solved with boundary conditions that ξ_{ij} go to zero for $z = 0$ and $z \rightarrow \infty$. This should be a good approximation for the SiO_2 -Si interface for which the potential barrier for electrons is approximately 3 eV. In the variational approximation technique presented here, the eigen energy are determined by using the trial envelope function considering the above boundary conditions.

The potential energy $V(z)$ which enters in equation (2.6) can be written as sum of the three terms as

$$V(z) = V_d(z) + V_s(z) + V_I(z) \quad (2.7)$$

Which represent, respectively, the contributions from fixed space charges (Depletion layer charges), from induced charges in the space charge layer (inversion layer charges), and from image charges at the semiconductor-insulator interface.

If the band bending ϕ_d associated with the depletion layer is not too small, if the bulk is p type, and if the acceptor density N_A is constant throughout the depletion layer, then a good approximation for the potential energy in the depletion layer is

$$V_d(z) = \frac{q^2 N_{\text{depl}}}{\epsilon_s} z \left(1 - \frac{z}{2Z_d} \right) ; \quad 0 < z < Z_d \quad (2.8)$$

With $N_{\text{depl}} = N_A Z_d$ (2.9)

Where N_{depl} is the number of charges per unit area in the depletion layer, whose thickness is Z_d and q is the electron charge. If compensating donors are present, N_A should be replaced by $N_A - N_D$. In most case of interest for silicon, the depletion layer is much wider than the inversion layer, and it is usually a good approximation to neglect the term quadratic in z in equation (2.8).

$V_s(z)$, the second term in equation (2.7) is the contribution to the potential energy from the charge distribution of the electrons in the space-charge layer, and is given by the solution of Poisson's equation with the charge density in all subbands as the source term. The Poisson's equation considering only the inversion layer charges,

$$\frac{d^2}{dz^2} V_s(z) = \frac{q^2}{\epsilon_s} \sum_{ij} N_{ij} \xi_{ij}^2(z) \quad (2.10)$$

The solution of equation (2.10) is

$$V_s(z) = \frac{q^2}{\epsilon_s} \sum_{ij} N_{ij} \left[z + \int_0^z (z' - z) \xi_{ij}^2(z') dz' \right] \quad (2.11)$$

Where N_{ij} is the electron concentration in the j th subband in the i th valley and $\xi_{ij}(z)$ is the corresponding normalized envelope wave function. The arbitrary constant of integration has been chosen to make $V_s(0) = 0$ and $\lim_{z \rightarrow \infty} \frac{dV_s(z)}{dz} = 0$.

The last term in the potential energy (2.7) is the image term

$$V_I(z) = \frac{\epsilon_s - \epsilon_{\alpha}}{\epsilon_s + \epsilon_{\alpha}} \frac{q^2}{16\pi z \epsilon_s} \quad (2.12)$$

Which arises because of the different dielectric constant of the semiconductor and the insulator. We will neglect this image term in all our calculations presented in this section. It is a good approximation at high carrier densities.

2.3.1 Ground state

Let, the trial envelope function for ground state,

$$\xi_{s_0}(z) = A z e^{-\frac{bz}{2}}$$

Considering the boundary conditions that, envelope function vanishes at $z = 0$ and $z \rightarrow \infty$. Here b is the undetermined parameter and A is a constant.

Normalization condition tells that,

$$\int_{-\infty}^{\infty} |\xi_{s_0}(z)|^2 dz = 1$$

$$\therefore \int_0^{\infty} A^2 z^2 e^{-bz} dz = 1$$

The value of A comes out, $A = \left(\frac{b^3}{2}\right)^{\frac{1}{2}}$

So, the normalized envelope function for ground state,

$$\xi_{10}(z) = \left(\frac{b^3}{2}\right)^{\frac{1}{2}} z e^{-\frac{bz}{2}} \quad (2.13)$$

The trial function of first excitation state is orthogonal to the envelope function of the ground state. Let, the trial envelope function for the first excited state

$$\xi_{11}(z) = Bz(1-Cz)e^{-\frac{bz}{2}}$$

Where B & C are arbitrary constants.

Orthogonal condition yields that,

$$\begin{aligned} \int_{-\infty}^{\infty} \xi_{10}^*(z) \xi_{11}(z) dz &= 0 \\ \therefore \int_0^{\infty} \left(\frac{b^3}{2}\right)^{\frac{1}{2}} Bz^2(1-Cz)e^{-bz} dz &= 0 \end{aligned}$$

From the above equation, $C = \frac{b}{3}$

Again the normalization condition yields,

$$\begin{aligned} \int_{-\infty}^{\infty} |\xi_{11}(z)|^2 dz &= 1 \\ \therefore \int_0^{\infty} B^2 z^2 \left(1 - \frac{b}{3}z\right)^2 e^{-bz} dz &= 1 \end{aligned}$$

From the above equation we get, $B = \left(\frac{3b^3}{2} \right)^{\frac{1}{2}}$

So, the normalized envelope function for first excited state is ,

$$\xi_{s1}(z) = \left(\frac{3b^3}{2} \right)^{\frac{1}{2}} z \left(1 - \frac{bz}{3} \right) e^{-\frac{bz}{2}} \quad (2.14)$$

In equilibrium and at the relatively high transverse fields existing in modern devices (even at zero gate drive), the lowest three energy levels are sufficient to account for most of the inversion layer charge [5]. It was found that adding higher subbands provided no discernible change in either the distribution or the total charge for positive gate biases and the channel doping levels ($\geq 10^{17} \text{ cm}^{-3}$) and oxide thickness (4 nm to 14 nm) considered there. The three lowest energy levels are in ascending order E_{10} , E_{20} , E_{11} and electron concentration in the three lowest subbands are in ascending order N_{10} , N_{20} and N_{11} .

Considering only the three lowest subbands, the equation (2.11) becomes ,

$$\begin{aligned} V_s(z) = & \frac{q^2}{\epsilon_s} N_{10} \left[z + \int_0^z (z' - z) \xi_{s10}^2(z') dz' \right] \\ & + \frac{q^2}{\epsilon_s} N_{20} \left[z + \int_0^z (z' - z) \xi_{s20}^2(z') dz' \right] \\ & + \frac{q^2}{\epsilon_s} N_{11} \left[z + \int_0^z (z' - z) \xi_{s11}^2(z') dz' \right] \end{aligned} \quad (2.15)$$

Let us assume that the envelope wave functions of ground state are same for both first and second valleys . i.e.

$$\xi_{10} = \xi_{20} = \left(\frac{b^3}{2}\right)^{\frac{1}{2}} z e^{-\frac{bz}{2}} \quad (2.16)$$

Integrating equation (2.15), we get,

$$\begin{aligned} V_s(z) = & \frac{q^2}{\epsilon_s} (N_{10} + N_{20}) \left\{ \frac{3}{b} - \frac{1}{2b} e^{-bz} (6 + 4bz + b^2 z^2) \right\} \\ & + \frac{q^2}{\epsilon_s} N_{11} \left\{ \frac{5}{b} - \frac{1}{b} e^{-bz} \left(5 + 4bz + \frac{3}{2} b^2 z^2 + \frac{1}{3} b^3 z^3 + \frac{1}{6} b^4 z^4 \right) \right\} \quad (2.17) \end{aligned}$$

The expectation value of $V_s(z)$ for ground state envelope function in the Hamiltonian,

$$\begin{aligned} \langle V_s \rangle &= \langle \xi_{10}(z) | V_s(z) | \xi_{10}(z) \rangle \\ &= \int_0^\infty V_s(z) |\xi_{10}(z)|^2 dz \end{aligned}$$

$$\therefore \langle V_s \rangle = \frac{33q^2}{16b\epsilon_s} (N_{10} + N_{20} + 1.1N_{11}) \quad (2.18)$$

Similarly, the expectation value of $V_d(z)$ in the Hamiltonian,

$$\langle V_d \rangle = \int_0^\infty V_d(z) |\xi_{10}(z)|^2 dz$$

Putting the value of $V_d(z)$ and $\xi_{10}(z)$ and integrating the above equation we get,

$$\langle V_d \rangle = \frac{3q^2 N_{\text{depl}}}{\epsilon_s b} - \frac{6q^2 N_{\text{depl}}}{\epsilon_s b^2 Z_d} \quad (2.19)$$

The expectation value of kinetic energy of an electron for ground state envelope function,

$$\begin{aligned} \langle T \rangle &= \frac{1}{2 m_{zi}} \int_0^\infty \left| \frac{\hbar}{i} \frac{\partial \xi_{10}(z)}{\partial z} \right|^2 dz \\ &= \frac{\hbar^2}{2 m_{zi}} \int_0^\infty \left(\frac{b^3}{2} \right)^{\frac{1}{2}} \left(e^{-\frac{bz}{2}} - \frac{b}{2} z e^{-\frac{bz}{2}} \right)^2 dz \\ &= \frac{\hbar^2 b^2}{8 m_{zi}} \\ \therefore \langle T \rangle &= \frac{\hbar^2 b^2}{8 m_{zi}} \quad (2.20) \end{aligned}$$

So, the mean value $\langle \mathbf{H} \rangle(b)$ of the Hamiltonian \mathbf{H} in the ground state,

$$\langle \mathbf{H} \rangle(b) = \langle T \rangle + \langle V_d \rangle + \langle V_s \rangle \quad (2.21)$$

However the total energy per electron, which is the quantity to be minimized is,

$$\frac{E}{N} = \langle T \rangle + \langle V_d \rangle + \frac{1}{2} \langle V_s \rangle$$

Where the factor $\frac{1}{2}$ prevents double counting of electron-electron interactions.

Neglecting second term in $\langle V_d \rangle$, We have,

$$\frac{E}{N} = \frac{\hbar^2 b^2}{8m_{zi}} + \frac{3q^2 N_{depl}}{\epsilon_s b} + \frac{33q^2}{32\epsilon_s b} (N_{10} + N_{20} + 1.1 N_{11}) \quad (2.22)$$

The value of b that minimizes the total energy per electron is

$$b = b_0 = \left[\frac{12m_{zi} q^2 N^*}{\epsilon_s \hbar^2} \right]^{\frac{1}{3}} \quad (2.23)$$

$$\text{Where, } N^* = N_{depl} + \frac{11}{32} (N_{10} + N_{20} + 1.1 N_{11})$$

The energy of the lowest subband is

$$\begin{aligned} E_{i0} &= \langle H \rangle (b_0) \\ &= \frac{\hbar^2 b_0^2}{8m_{zi}} + \frac{3q^2 N_{depl}}{b_0 \epsilon_s} + \frac{33q^2}{16\epsilon_s b_0} (N_{10} + N_{20} + 1.1 N_{11}) \\ &= \left(\frac{3}{2} \right)^{\frac{5}{3}} \left(\frac{q^2 \hbar^2}{\epsilon_s m_{zi}^{\frac{1}{2}}} \right)^{\frac{2}{3}} \frac{N^{**}}{(N^*)^{\frac{1}{3}}} \end{aligned}$$

$$\text{Where, } N^{**} = N_{depl} + \frac{55}{96} (N_{10} + N_{20} + 1.1 N_{11})$$

Thus we have,

$$E_{10} = \left(\frac{3}{2}\right)^{\frac{5}{3}} \left(\frac{q^2 \hbar^2}{\epsilon_s m_{z1}^2}\right)^{\frac{2}{3}} \frac{N^{**}}{(N^*)^{\frac{1}{3}}} \quad (2.24)$$

$$E_{20} = \left(\frac{3}{2}\right)^{\frac{5}{3}} \left(\frac{q^2 \hbar^2}{\epsilon_s m_{z2}^2}\right)^{\frac{2}{3}} \frac{N^{**}}{(N^*)^{\frac{1}{3}}} \quad (2.25)$$

2.3.2 Excited energy state

The envelope wave function for the first excited state of first valley is [from equation 2.14]

$$\xi_{11}(z) = \left(\frac{3b^3}{2}\right)^{\frac{1}{2}} z \left(1 - \frac{bz}{3}\right) e^{-\frac{bz}{2}}$$

The expectation value of kinetic energy for the envelope wave function $\xi_{11}(z)$ is,

$$\langle T \rangle = \frac{1}{2m_{zi}} \int_0^\infty \left| \frac{\hbar}{i} \frac{\partial}{\partial z} \xi_{11}(z) \right|^2 dz$$

$$\therefore \langle T \rangle = \frac{7b^2 \hbar^2}{24m_{zi}} \quad (2.26)$$

The expectation value of $V_d(z)$ for the envelope wave function $\xi_{11}(z)$ is ,

$$\begin{aligned}\langle V_d \rangle &= \int_0^\infty V_d(z) |\xi_{11}(z)|^2 dz \\ \therefore \langle V_d \rangle &= \frac{5q^2 N_{\text{depl}}}{\epsilon_s b} \left(1 - \frac{3.6}{z_d b} \right)\end{aligned}\quad (2.27)$$

The expectation value of $V_s(z)$ for the envelope wave function $\xi_{11}(z)$ is

$$\begin{aligned}\langle V_s \rangle &= \int_0^\infty V_s(z) |\xi_{11}(z)|^2 dz \\ \therefore \langle V_s \rangle &= \frac{73q^2}{32b\epsilon_s} (N_{10} + N_{20} + 1.37N_{11})\end{aligned}\quad (2.28)$$

So, the mean value $\langle H \rangle(b)$ of the Hamiltonian H in the first excited state of first valley,

$$\begin{aligned}\langle H \rangle(b) &= \langle T \rangle + \langle V_d \rangle + \langle V_s \rangle \\ \therefore \langle H \rangle(b) &= \frac{7\hbar^2 b^2}{24m_{zi}} + \frac{5q^2 N_{\text{depl}}}{b\epsilon_s} \left(1 - \frac{3.6}{z_d b} \right) + \frac{73q^2}{32b\epsilon_s} (N_{10} + N_{20} + 1.37N_{11})\end{aligned}$$

This function for the same value of b_0 as above (equation 2.23) , presents a minimum equal to

$$E_{11} = \frac{7\hbar^2 b_0^2}{24m_{zi}} + \frac{5q^2 N_{\text{depl}}}{b_0 \epsilon_s} \left(1 - \frac{3.6}{z_d b_0} \right) + \frac{73q^2}{32b_0 \epsilon_s} (N_{10} + N_{20} + 1.37N_{11}) \quad (2.29)$$

putting the value of b_0 and neglecting the second term of $\langle V_d \rangle$, the expression of E_{11} becomes,

$$E_{11} = \left(\frac{17}{2} \right) \left(\frac{1}{12} \right)^{\frac{1}{3}} \left(\frac{q^2 \hbar^2}{\epsilon_s m_z \frac{1}{2}} \right)^{\frac{2}{3}} \frac{N^{***}}{(N^*)^{\frac{1}{3}}} \quad (2.30)$$

where, $N^{***} = N_{\text{depl}} + 0.41(N_{10} + N_{20} + 1.28N_{11})$

2.4 Conclusions

In this chapter, the analytical expressions of the ground state eigen energies for two valleys and the first excited state eigen energy for first valley of inversion MOS structure are derived using the variational approximation technique. The eigen functions for various subbands are assumed considering the physical criteria of the system. Knowing the energy and wavefunction of energy-bands, electron population and other parameters for characterizing the inversion layer MOS structure can be obtained in next chapter.

CHAPTER 3

ANALYSIS FOR FREQUENCY DEPENDENCE OF TOTAL GATE CAPACITANCE

3.1 Introduction

It is well known that the electrons of the MOS inversion layer form subbands, each of which corresponds to a quantized level for motion in the direction perpendicular to the silicon-insulator surface. In chapter two, eigen values of first three consecutive subbands of inversion MOS structure are determined by applying variational approximation method.

In this chapter, the electron charges in the three subbands are determined as a function of Fermi energy and subband energies with the help of Fermi-Dirac statistical distribution law. The total electron charges within the inversion layer is considered as the sum of electron charges in the three first consecutive subbands. Knowing the carrier concentration in the subbands, an analytical expression for capacitance is determined by simply differentiating the total charge in the inversion layer with respect to the Fermi potential, in contrary to

the conventional method. In conventional approach the charges are differentiated with respect to surface potential. To find the dependence on capacitance, the thermally generated electrons within the depletion region and the flow of electrons from the bulk to the SiO₂-Si interface need to be incorporated in quantum capacitance calculated from energy subbands. The approximate equivalent circuit of MOS structure is determined by following step by step the flow of charges (electrons and holes) from the bulk of the semiconductor to the SiO₂-Si interface. In Each step, the rate of flow of charges is limited by its resistance. Accumulation of charges can be associated with a capacitor. Resistances are calculated using the standard equations for finding the resistances in the semiconductor. In chapter one, the oxide capacitance and the depletion capacitance are expressed using the classical method for finding the capacitance. Finally, from the equivalent circuit of MOS structure, the analytical expression for the frequency dependence of total gate capacitance of inversion MOS structure is determined here in this chapter.

3.2 Charge concentration in three subbands

The density of states for a two-dimensional system is constant and is given by the following equation [5],

$$D(E) = \frac{2n_{vi}m_{di}}{2\pi\hbar^2} \quad (3.1)$$

Where n_{vi} and m_{di} are the valley degeneracy factor and the density-of-states effective mass per valley. the degeneracy is taken care of by the factor $2n_{vi}$, where n_{vi} is the number of equivalent energy surfaces and the factor two represents an additional degeneracy due to electron spin. The occupancy n_{ij} (jth subband in the ith valley) is defined through Fermi-Dirac statistics by

$$N_{ij} = \int_{E_{ij}}^{\infty} D(E) f_{FD}(E) dE \quad (3.2)$$

Where $f_{FD}(E)$ is the Fermi-Dirac distribution function which is given by

$$f_{FD}(E) = \frac{1}{1 + e^{\frac{(E-E_F)}{kT}}} \quad (3.3)$$

$$\text{So, } N_{ij} = \frac{n_{vi} m_{di}}{\pi \hbar^2} \int_{E_{ij}}^{\infty} \frac{1}{1 + e^{\frac{(E-E_F)}{kT}}} dE$$

$$\therefore N_{ij} = \frac{n_{vi} m_{di} kT}{\pi \hbar^2} \ln \left\{ 1 + e^{\frac{-(E_{ij}-E_F)}{kT}} \right\} \quad (3.4)$$

The total inversion layer charge

$$N_{inv} = \sum_{ij} N_{ij} \quad (3.5)$$

is the total number of charges per unit area in the inversion layer

3.3 Surface potential and related equations considering quantum mechanical effects

The electric field at the Si-SiO₂ interface is given by

$$F_s = \frac{q(N_{inv} + N_{depl})}{\epsilon_s} \quad (3.6)$$

$$\text{Where, } N_{\text{depl}} = N_A Z_d \quad (3.7)$$

$$\text{and } Z_d = \sqrt{\frac{2\epsilon_s \phi_d}{qN_A}} \quad (3.8)$$

Here, N_{depl} is the concentration of depletion layer charge, ϵ_s is the permittivity of semiconductor, Z_d is the width of the depletion layer and ϕ_d is the surface potential due to depletion region ionized acceptors.

The surface potential ψ_s arises from the contribution of both the depletion and inversion layer charges. Since the bottom of the conduction band is taken as zero at the Si-SiO₂ interface we have [fig 3.1]

$$q\psi_s = (E_c - E_F)_b + E_F \quad (3.9)$$

Where $(E_c - E_F)_b$ is the energy difference between the bottom of the conduction band in the bulk and the Fermi level and E_F is the Fermi energy relative to the nominal conduction band edge at the surface. $(E_c - E_F)_b$ is given by

$$(E_c - E_F)_b = E_g - kT \ln \frac{N_v}{N_A} \quad (3.10)$$

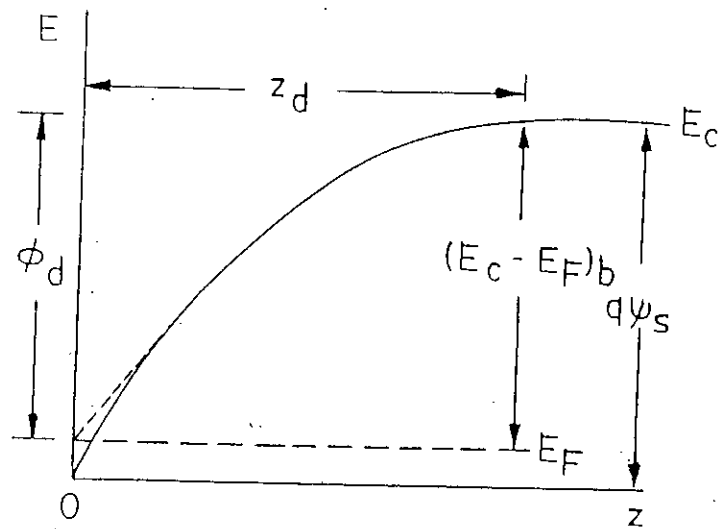
Where N_v is the effective density of states in the valence band .

Now, the contribution of inversion layer electrons to the surface potential can be written as

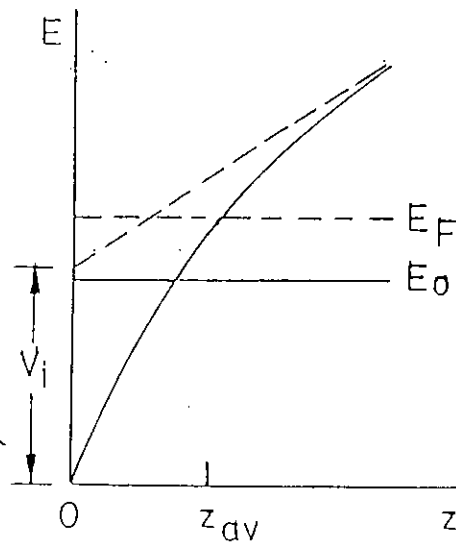
$$V_i = \frac{qN_{\text{inv}}Z_{\text{av}}}{\epsilon_s} \quad (3.11)$$

Where, Z_{av} is the average distribution of inversion layer from the semiconductor- insulator interface which is given by

$$Z_{\text{av}} = \sum_{ij} \frac{N_{ij}Z_{ij}}{N_{\text{inv}}} \quad (3.12)$$



(a)



(b)

Fig. 3.1 Schematic band bending due to depletion and inversion layer charges (solid line) and corresponding band bending associated with the fixed depletion layer charges only (dashed line).

(a) Surface potential ψ_s and band bending

(b) Potential drop due to inversion charges

$$\text{where } Z_{ij} = \frac{\int_0^{\infty} z \xi_{ij}^2(z) dz}{\int_0^{\infty} \xi_{ij}^2(z) dz} \quad (3.13)$$

is the average distance from the semiconductor- insulator interface of electrons of the j th subband in the i th valley.

It is usually assumed that the depletion charge is constant for a distance Z_d , the depletion layer width, from the surface and then goes abruptly zero. This assumption fails in the transition region from depletion to bulk, in which the field decays to zero exponentially with a characteristic distance given by the bulk screening length. When the correction to ϕ_d is taken to be $-\frac{kT}{q}$ [6],

$$q\phi_d = \left[(E_c - E_F)_b + E_F - kT \right] - \frac{N_{inv} Z_{av}}{\epsilon_s} \quad (3.14)$$

Where, k is the Boltzmann's constant and T is the absolute temperature.

The gate voltage V_G can be written as

$$V_G = V_{ox} + \psi_s + V_{FB} \quad (3.15)$$

$$\text{Where, } V_{ox} = \frac{\epsilon_s F_s d}{\epsilon_{ox}} \quad (3.16)$$

is the oxide layer voltage drop, F_s is the normal electric field at $\text{SiO}_2\text{-Si}$ interface, d is the oxide layer thickness and ϵ_{ox} is the permittivity of the oxide. V_{FB} is the flat-band voltage. If we neglect charges in the oxide, then V_{FB} is the required gate voltage due to the difference of work functions between Si and metal contact.

3.4 Analytical expression for inversion layer quantum capacitance

Inversion layer quantum capacitance per unit area is denoted by

$$C_I = - \frac{dQ_{inv}}{d\psi_s} \quad (3.17)$$

Q_{inv} is total charge in the inversion layer and ψ_s is the surface potential .

putting $Q_{inv} = -q N_{inv}$ in equation (3.17) we have ,

$$C_I = q \frac{dN_{inv}}{d\psi_s} \quad (3.18)$$

It can be written as ,

$$C_I = q \frac{dN_{inv}}{dE_F} \cdot \frac{dE_F}{d\psi_s} \quad (3.19)$$

Differentiating equation (3.9) w.r.t ψ_s we get,

$$\frac{dE_F}{d\psi_s} = q \quad (3.20)$$

putting the value of $\frac{dE_F}{d\psi_s}$ in equation (3.19), we have

$$C_I = q^2 \frac{dN_{inv}}{dE_F} \quad (3.21)$$

From equation (3.4), (3.5) and (3.21), we have

$$C_I = \frac{q^2}{\pi \hbar^2} \sum_{ij} \frac{n_{vi} m_{di}}{1 + e^{\frac{(E_{ij} - E_F)}{kT}}} \quad (3.22)$$

Considering only first three consecutive subbands,

$$C_I = \frac{q^2}{\pi \hbar^2} \left\{ \frac{n_{v1} m_{d1}}{1 + e^{\frac{(E_{10} - E_F)}{kT}}} + \frac{n_{v2} m_{d2}}{1 + e^{\frac{(E_{20} - E_F)}{kT}}} + \frac{n_{v1} m_{d1}}{1 + e^{\frac{(E_{11} - E_F)}{kT}}} \right\} \quad (3.23)$$

Thus the inversion layer quantum capacitance depends on the eigen energies, Fermi energy, valley degeneracy and the density-of-states effective mass per valley.

3.5 Frequency dependence of total gate capacitance of submicron inversion MOS structure

In the inversion mode of operation of MOS structure, a thin inversion layer near SiO₂-Si interface is formed. There are several sources which can supply the minority carriers required to change the charge in the inversion layer and a current can be associated with each source. Lehovc and Slobodskoy [16,17] have proposed an equivalent circuit for the input impedance of the MOS capacitor in the bias range for depletion-inversion. This circuit is reproduced in Fig.3.2, with the notation appropriate to a p-type substrate.

The equivalent circuit of Fig. 3.2 is given by following step by step the flow of charges (electrons and holes) from the bulk of the semiconductor to the SiO₂-Si interface. In each step, the rate of flow of charges is limited by its resistance. Accumulation of charges can be associated with capacitors.

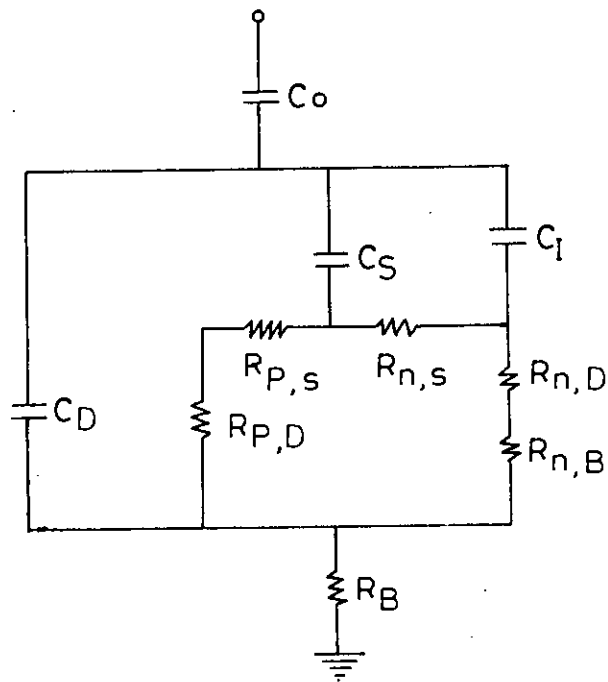


Fig. 3.2 Equivalent circuit for p-type MOS capacitor in depletion-inversion mode after Lehavec and Slobodsky [Ref. 16].

Since changes of charge in surface states with time involve flow of electrons or holes through the space-charge layer, the rate of these changes will be limited by the a.c voltage across the space-charge layer, by its conductance and by the transition rates of carriers from the conduction band and valence band to the surface states. C_0 is the capacitance of the oxide and is supplied by the displacement current of C_D and by the flow of electrons between the bulk and the inversion layer. There are two resistances associated with this latter flow. One is $R_{n,B}$, associated with the diffusion current of electrons from the bulk to the edge of the depletion region. The other is $R_{n,D}$, associated with the electron current through the depletion region to the surface.

C_s is the surface state capacitance supplied by the flow of holes between the valence band and the surface states and by the flow of electrons between the conduction band and the surface states. The resistances associated with these two flows are $R_{p,s}$ and $R_{n,s}$ respectively. In addition, there is a resistance $R_{p,D}$ associated with the flow of holes from the bulk to the surface, and a resistance R_B which is simply the bulk resistance of the semiconductor.

C_1 is the inversion layer capacitance, which is supplied by a flow of electrons between the inversion layer and the surface states and by a flow of electrons from the bulk through the depletion layer. C_D is the capacitance associated with majority carrier motion at the bulk edge of the depletion region.

In the heavy inversion mode, the circuit may be simplified considerably to that shown in Fig. 3.3a, an additional source of carriers to the inversion layer, not considered by Lehovec and Slobodskoy, is finite generation and

recombination with in the space charge layer. The resistance associated with this current is defined as R_{gD} and appears across the combination $R_{n,B} + R_{n,D}$. The physical basis for these simplifications are presented in the following discussions.

(i) The bulk resistance R_B , will be neglected in the analysis, since it does not affect directly the frequency response of the inversion layer.

(ii) Due to the quantum mechanical nature of 2DEG, the distribution of carriers follow the curve of Fig.1.5 and there is no carriers in SiO_2 -Si interface. So, we can neglect all parameters of Fig.3.2 related to the surface states.

Thus, the resulting simplified equivalent circuit is shown in Fig. 3.3a.

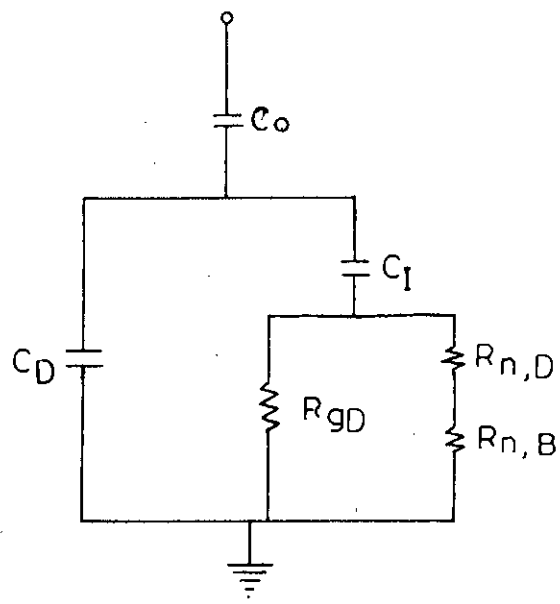
For frequencies substantially below the inverse of minority carrier lifetime, the bulk diffusion resistance $R_{n,B}$ is given by [Appendix I],

$$R_{n,B} = \frac{(D_n \tau_n)^{\frac{1}{2}}}{q\mu_n N_A} \quad (3.24)$$

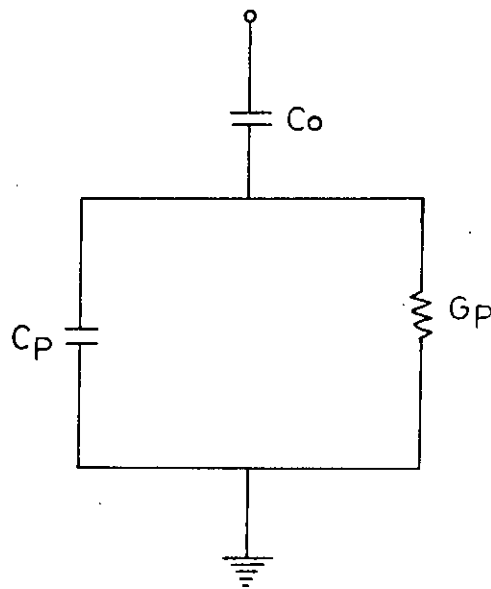
D_n is the diffusion coefficient of electron, μ_n is the mobility of electron and τ_n is the minority carrier lifetime in the bulk.

The resistance $R_{n,D}$ is associated with the flow of minority carriers through the depletion layer. It is shown in Appendix II that

$$\frac{R_{n,B}}{R_{n,D}} \gg 1 \quad (3.25)$$



(a)



(b)

Fig. 3.3 Simplified equivalent circuit for p-type MOS capacitor with heavy inversion layer.

Therefore, we can neglect the depletion layer resistance $R_{n,D}$ in our equivalent circuit so that resistance associated with electron diffusion current from the bulk, $R_d = R_{n,B}$.

The resistance associated with the generation recombination in the depletion region is given by [Appendix III],

$$R_{gd} = \frac{2\tau_0\phi_d}{qn_iZ_d} \quad (3.26)$$

From the simplified equivalent circuit of Fig.3.3a, it is seen that $R_{n,B}$ and R_{gd} are in parallel. So, the equivalent value of resistance R is given by,

$$R = \frac{R_{gd}R_{n,B}}{R_{gd} + R_{n,B}} \quad (3.27)$$

Therefore, the series combination of quantum capacitance C_I and resistance R are in the parallel with depletion capacitance C_D . From Fig. 3.3a, these combinations can be written as an equivalent admittance,

$$Y'_{in} = j\omega C_p + G_p \quad (3.28)$$

$$\text{Where, } C_p = C_D + \frac{C_I}{1 + \omega^2\tau^2} \quad (3.29)$$

$$\text{and } G_p = \frac{C_I\omega\tau}{1 + \omega^2\tau^2} \quad (3.30)$$

ω is the angular frequency and $\tau = R C_I$.

So, the equivalent circuit of Fig. 3.3a can be redrawn in Fig. 3.3b in more simplified form. From Fig. 3.3b, the input admittance of MOS capacitor can be written as

$$Y_G = j \omega C_G + G_G \quad (3.31)$$

$$\text{Where, } G_G = \frac{\omega^2 R C_I^2 C_0^2}{(C_I + C_0 + C_D)^2 + \omega^2 R C_I (C_0 + C_D)^2} \quad (3.32)$$

$$\text{and } C_G = \frac{C_0}{C_0 + C_D + C_I} \left\{ C_D + C_I \frac{1 + (\frac{\omega}{\omega_c})^2}{1 + (\frac{\omega}{\omega_c})^2 (1 + \frac{C_0}{C_D})} \right\} \quad (3.33)$$

ω_c is the cut-off frequency . It is the transition frequency from the low to high frequency behavior of MOS capacitor. The expression of ω_c can be written as

$$\omega_c = \frac{C_0 + C_D + C_I}{R C_I \sqrt{C_D (C_0 + C_D)}} \quad (3.34)$$

So, the analytical expression of frequency dependence of total gate capacitance can be written as,

$$C_G = \frac{C_0}{C_0 + C_D + C_I} \left\{ C_D + C_I \frac{1 + (\frac{\omega}{\omega_c})^2}{1 + (\frac{\omega}{\omega_c})^2 (1 + \frac{C_0}{C_D})} \right\} \quad (3.35)$$

For $\omega \ll \omega_c$

$$C_G = \frac{C_0 (C_D + C_I)}{C_0 + C_D + C_I} = \frac{1}{\frac{1}{C_0} + \frac{1}{C_D + C_I}} \quad (3.36)$$

While for $\omega \gg \omega_c$

$$C_G = \frac{C_0 C_D}{C_0 + C_D} = \frac{1}{\frac{1}{C_0} + \frac{1}{C_D}} \quad (3.37)$$

Thus the total gate capacitance at low frequencies follows the equation (3.36) and at high frequencies the total gate capacitance follows the equation (3.37).

3.6 Conclusions

In this chapter, analytical expressions for inversion layer quantum capacitance and the frequency dependence of total gate capacitance of inversion MOS structure are derived. The populations of electrons in three-subbands are determined using density of states and Fermi-Dirac statistics. The total charges in the inversion layer depend upon the values of Fermi energy and the subband energies. Knowing the carrier concentration in the subbands, an analytical expression for inversion layer quantum capacitance is determined by simply differentiating the total charge in the inversion layer with respect to the Fermi potential. The approximate equivalent circuit for determining the impedance of MOS structure is obtained following step by step the flow of charges (electrons and holes) from the bulk of the semiconductor to the SiO₂-Si interface. From the equivalent circuit of MOS structure, the analytical expression for the frequency dependence of total gate capacitance of inversion MOS structure is determined. The results based on analytical solutions of this chapter and the comparison

study between the results of classical and quantum mechanical analysis are given in the next chapter.

CHAPTER 4

RESULTS AND DISCUSSIONS

4.1 Introduction

Based on the mathematical model developed in chapter two and chapter three, the frequency dependence of total gate capacitance is studied in this chapter using computational method. In chapter two, the analytical expressions of first three consecutive subbands are derived. The analytical model for quantum capacitance and frequency dependence of total gate capacitance considering quantum effects are obtained in chapter three. The eigen energies, the inversion layer carrier concentrations, the carrier concentration in the three consecutive subbands, the inversion layer quantum capacitance and the frequency dependence of total gate capacitance for different channel doping levels are studied in this chapter. Also, in this chapter, inversion layer quantum capacitance and the total gate capacitance considering the quantum mechanical effects are compared with that of the classical one. All studies are performed at 300°K for a (100) surface of p-type silicon substrate with a gate oxide thickness of 4 nm . The parameters required for computational studies are taken from table I .

TABLE I. Parameters used in the calculation.^a

Surface		(100)	
Valleys		Lower	Higher
Degeneracy	n_v	2	4
Normal mass	m_z	0.916	0.190
Density of states			
mass (per valley)	m_d	0.190	0.417

^aAll effective masses are in units of the free-electron mass (Courtesy Ref . 6)

4.2 Subbands energies

The predicted energy levels (with the bottom of conduction band at Si-SiO₂ interface is considered as reference level zero) of the lower two subbands in the first valley (E_{10} and E_{11}) and one subband in the higher valley for MOS capacitor with a uniform channel doping of $N_A=1.1 \times 10^{24} \text{ m}^{-3}$ are shown in Fig. 4.1 , 4.2 , 4.3 and 4.4 . The energy levels of the lowest three subbands (E_{10} , E_{20} and E_{11}) increases as the device becomes more strongly inverted.

The energy levels of first three consecutive subbands (E_{10} , E_{20} and E_{11}) for three channel doping are shown in Fig. 4.5 and Fig. 4.6 . The doping values corresponding to three sets of data are $1.0 \times 10^{23} \text{ m}^{-3}$, $5.0 \times 10^{23} \text{ m}^{-3}$ and $1.1 \times 10^{24} \text{ m}^{-3}$ respectively. The variation of energy levels E_{10} and E_{20} with the variation of channel doping is small and it decreases as the device becomes more strongly inverted. But there exists considerable variation in the energy level E_{11}

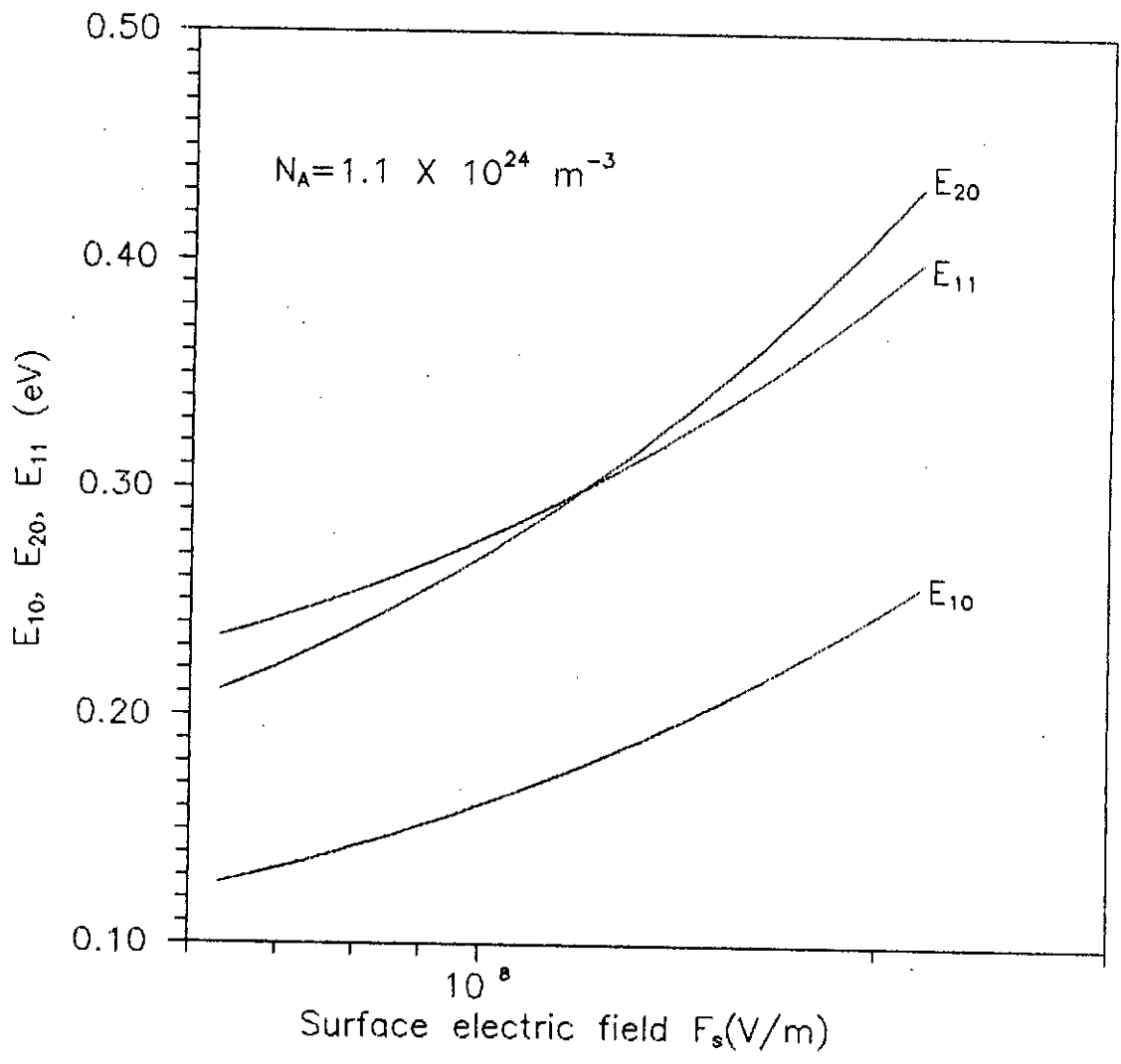


Fig. 4.1 Effect of surface electric field on the subband energy levels

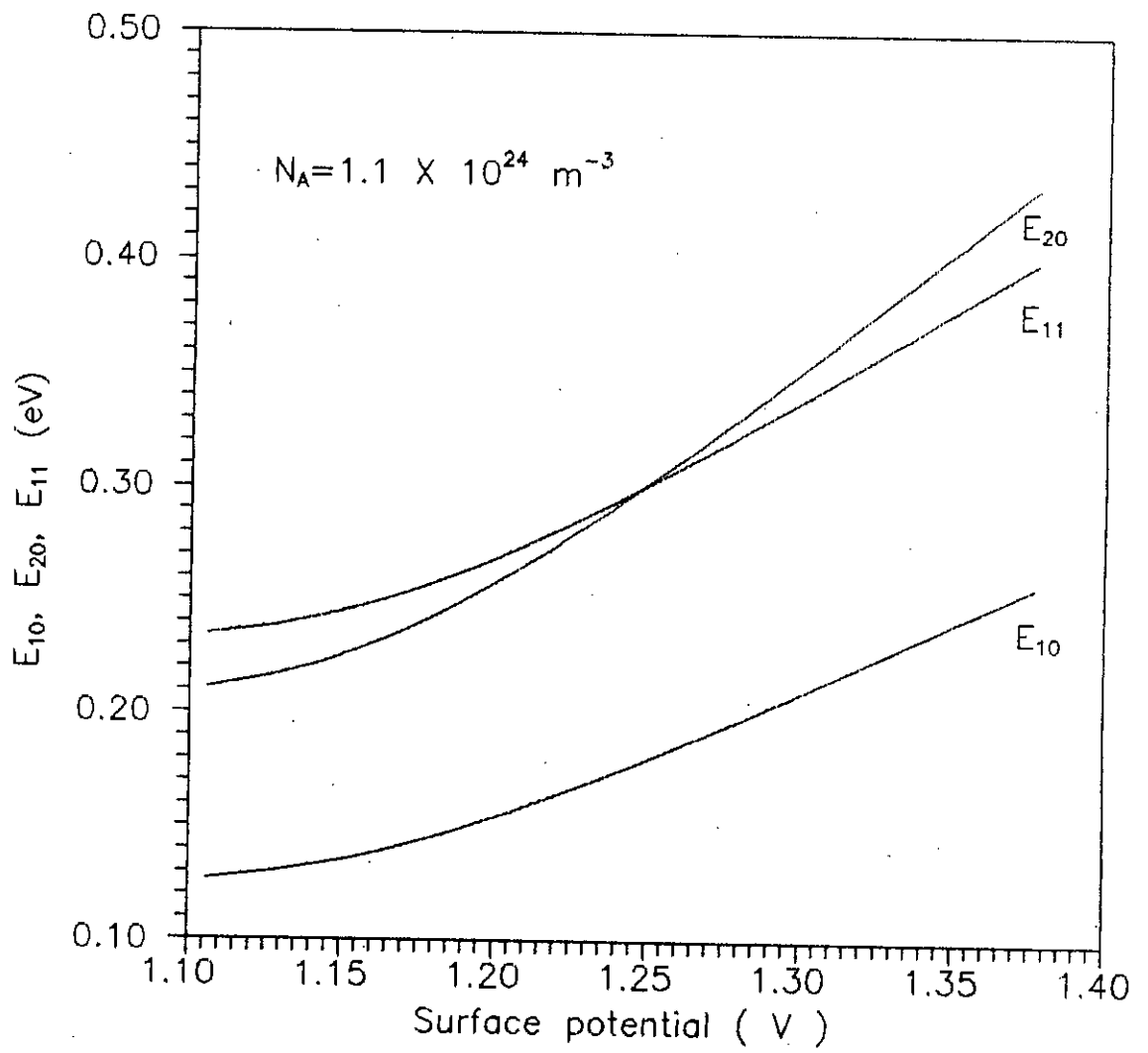


Fig. 4.2 Effect of surface potential on the subband energy levels

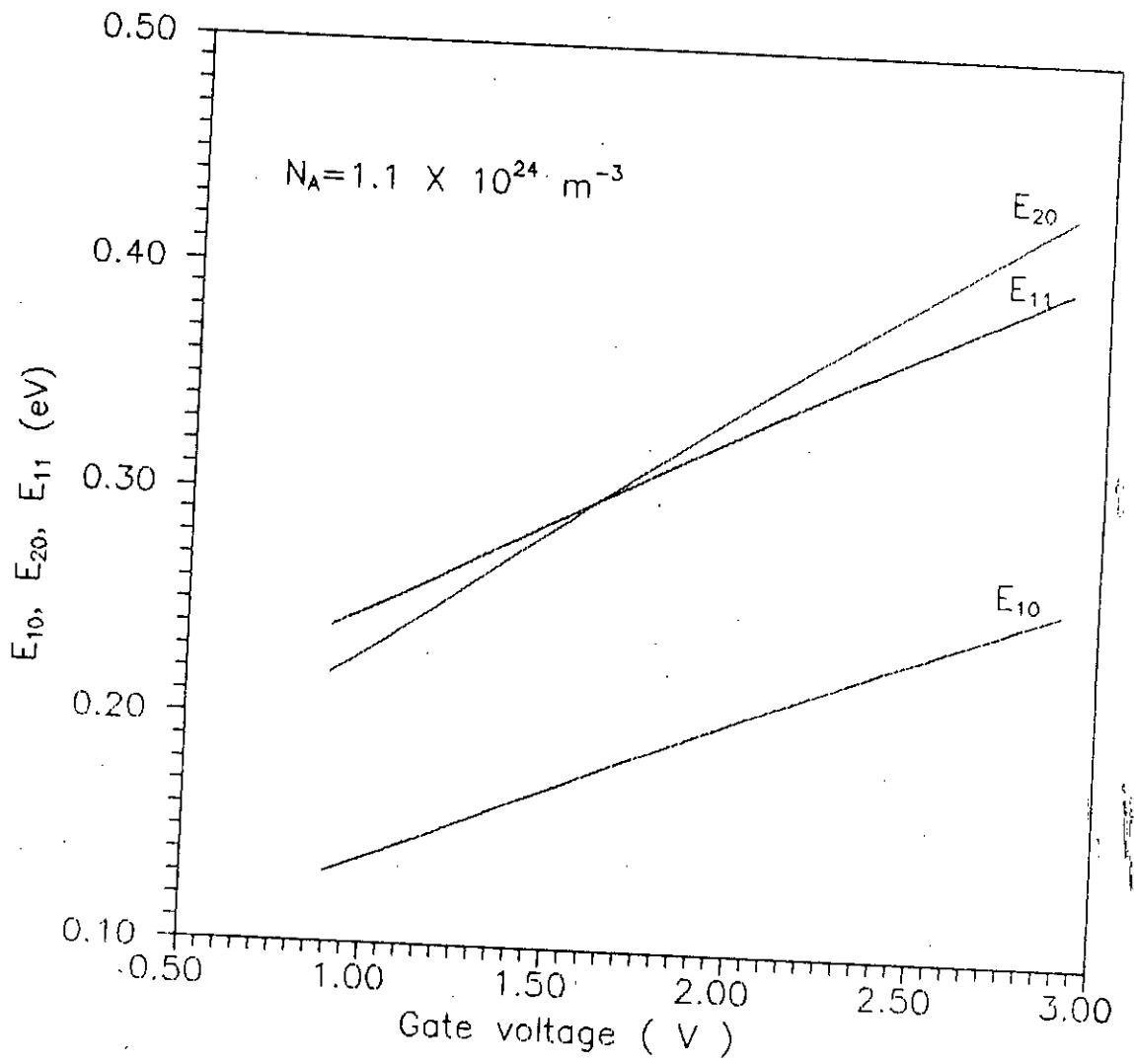


Fig. 4.3 Effect of gate voltage on the subband energy levels

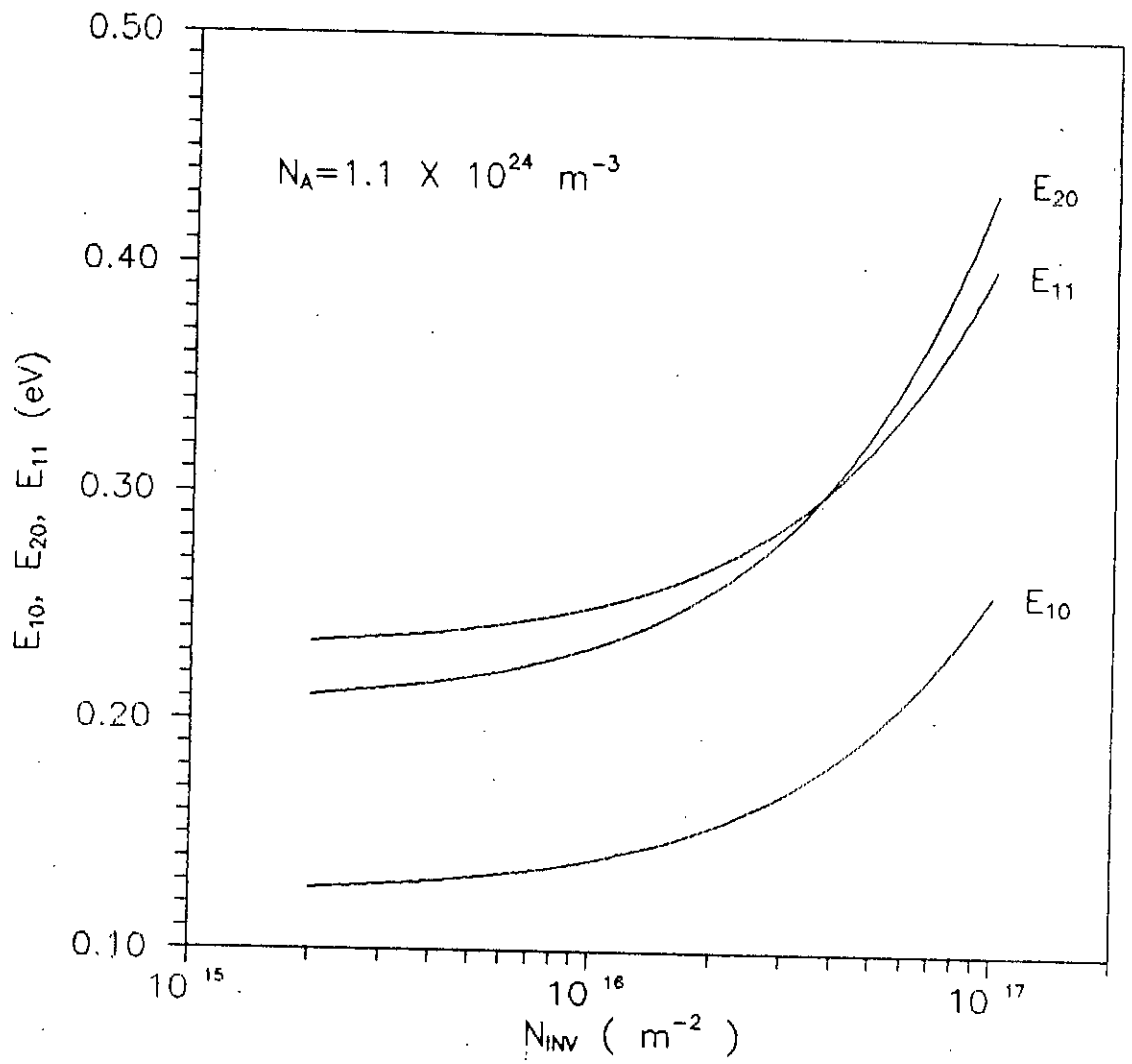


Fig. 4.4 Effect of inversion layer charge on the subband energy levels

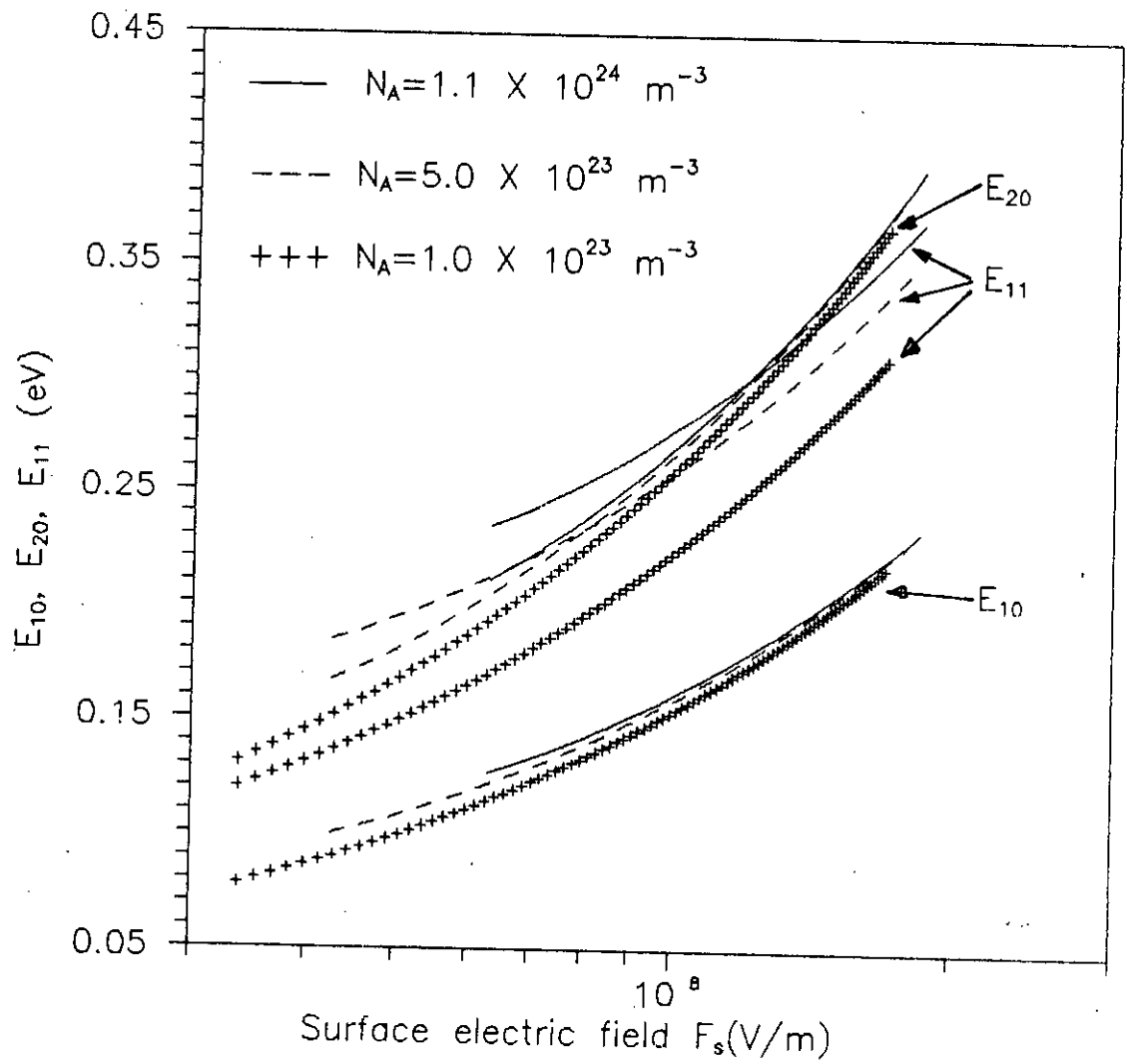


Fig 4.5 Subband energy levels vs. surface electric field for three different channel doping

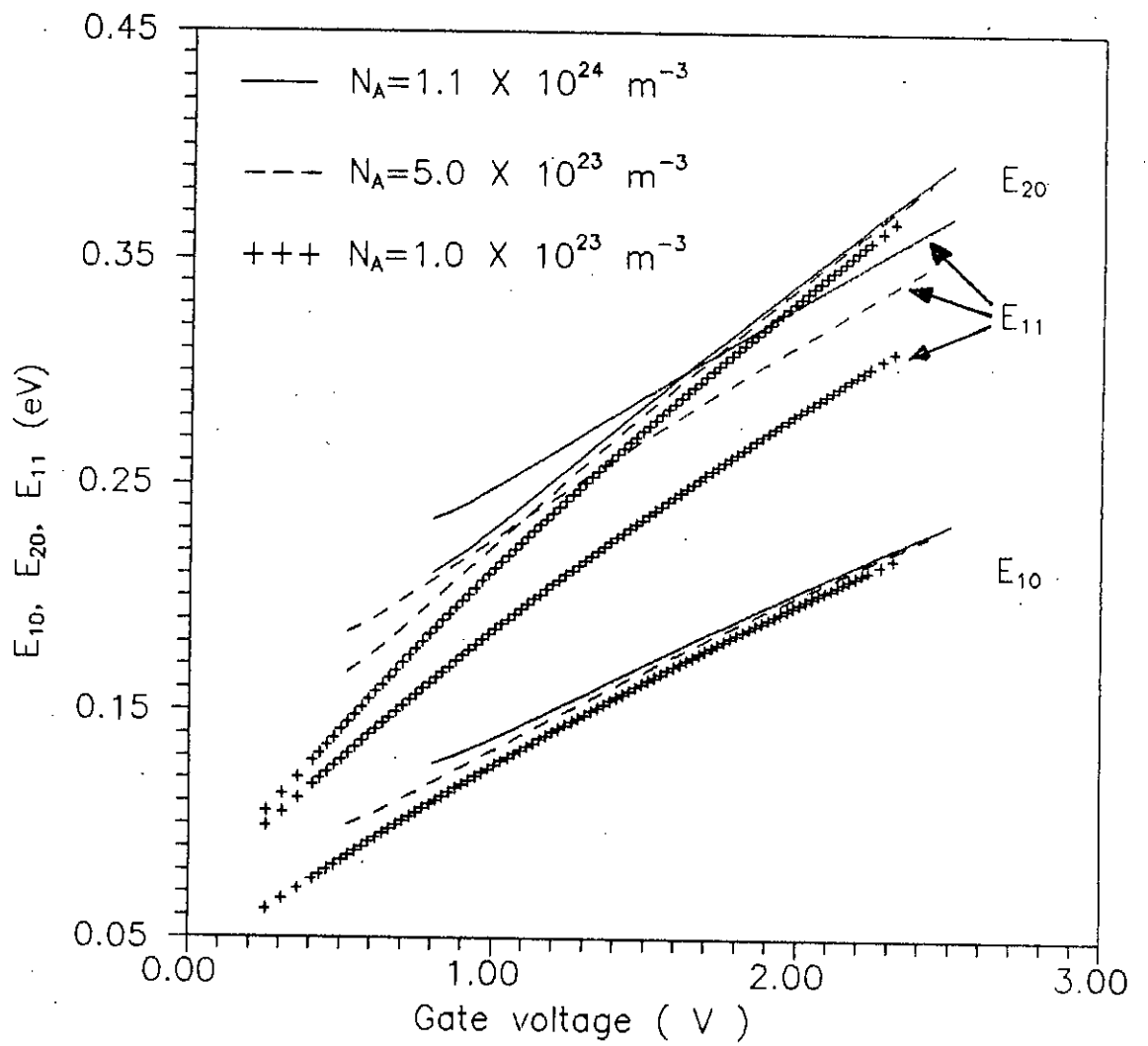


Fig. 4.6 Subband energy levels vs. gate voltage for three different channel doping

with the variation of channel doping. For a fixed electric field at the $\text{SiO}_2\text{-Si}$ interface the total charge concentration (depletion plus inversion layer charge) is also fixed and the concentration of depletion layer charge increases considerably with the increase of channel doping. It is found from expression (2.29) that contribution of depletion layer charge (N_{depl}) to the value of energy E_{11} is almost two times greater than inversion layer charge. Thus the value of energy E_{11} increases considerably with the increase of channel doping.

4.2.1 Comparison with self-consistent results

The self-consistent calculations results[11] of energy levels of first three consecutive subbands (E_{10} , E_{20} and E_{11}) are given in Fig 4.7 for a (100) surface of p-type silicon at 300°K with a gate oxide thickness of 4 nm and with a uniform channel doping of $N_A=1.1 \times 10^{24} \text{ m}^{-3}$. The comparison of variational and self-consistent [11] values of energies E_{10} , E_{20} and E_{11} as a function of gate voltage are given in tableII. It is seen that there is very small difference between the energy levels computation using variational approximation method and the self-consistent results. The results of the variational approximation agree well with the self-consistent calculation[11].

The determination of energy levels using self-consistent calculation are very accurate. But self-consistent solution of Schrodinger's and Poisson's equations requires iterative numerical procedures. Numerical calculations require considerable computational effort and it is very time consuming. But almost the same results can be obtained by using variational method. The main advantage of using this method is that it gives analytical solutions and requires very small computational time. The other important advantage is that it reveals the contribution of different parameters on the subband energies.

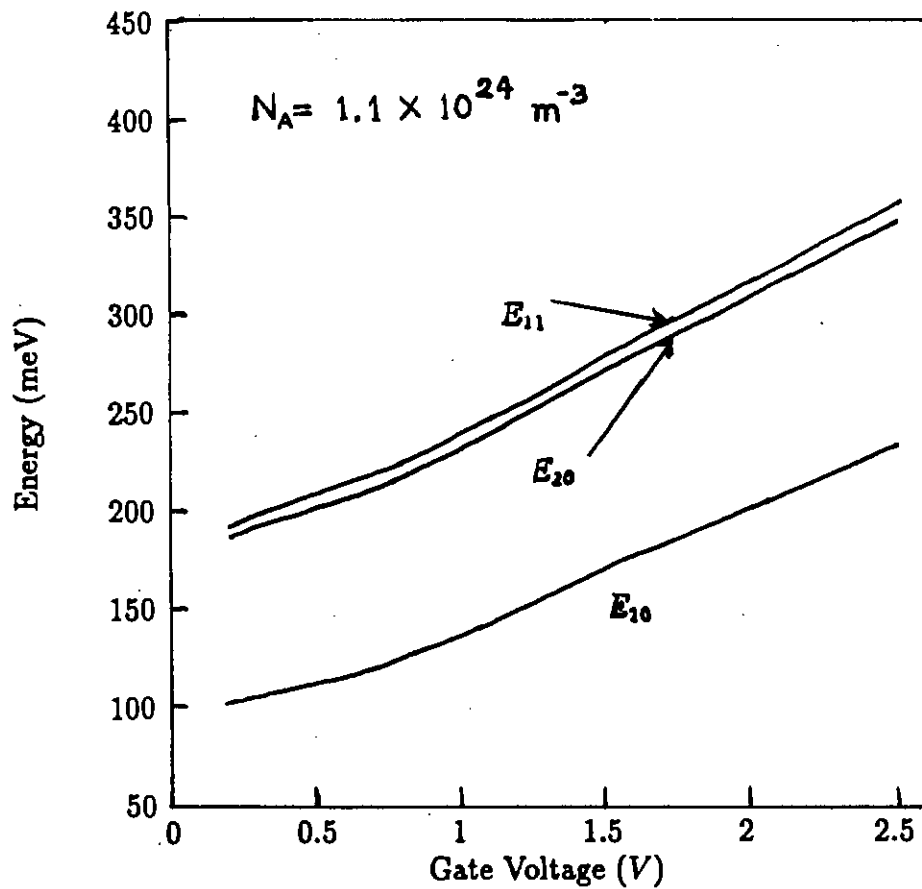


Fig. 4.7 Subband energy levels vs. gate voltage characteristics calculated self-consistently (Courtesy, Ref. 11)

TABLE II: Comparison of variational (var) and self-consistent (sc)[Ref. 11] values of energies E_{10} , E_{20} and E_{11} as a function of gate voltage (V_G) for channel doping of $N_A = 1.1 \times 10^{24} \text{ m}^{-3}$. All energies are in eV.

V_G (volt)	E_{10} (var)	E_{10} (sc)	E_{20} (var)	E_{20} (sc)	E_{11} (var)	E_{11} (sc)
0.8	0.126	0.126	0.212	0.220	0.231	0.227
0.9	0.131	0.131	0.219	0.227	0.240	0.234
1.0	0.137	0.137	0.230	0.234	0.247	0.241
1.1	0.143	0.144	0.241	0.241	0.255	0.248
1.2	0.150	0.151	0.251	0.249	0.263	0.256
1.3	0.157	0.158	0.263	0.256	0.271	0.264
1.4	0.163	0.164	0.274	0.264	0.281	0.270
1.5	0.170	0.170	0.286	0.271	0.289	0.276
1.6	0.176	0.177	0.296	0.276	0.296	0.285
1.7	0.183	0.182	0.306	0.285	0.305	0.294
1.8	0.189	0.188	0.319	0.294	0.313	0.302
1.9	0.196	0.196	0.329	0.302	0.322	0.309
2.0	0.202	0.203	0.339	0.309	0.329	0.315
2.1	0.208	0.209	0.350	0.315	0.337	0.324
2.2	0.214	0.215	0.360	0.324	0.345	0.333
2.3	0.220	0.221	0.371	0.333	0.353	0.342
2.4	0.227	0.227	0.381	0.342	0.361	0.349
2.5	0.235	0.235	0.391	0.349	0.368	0.357

4.3 Inversion layer carrier concentration

The inversion layer carrier concentration calculated quantum mechanically for channel doping $N_A=1.1 \times 10^{24} \text{ m}^{-3}$ as a function of surface potential (ψ_s) and gate voltage (V_G) are shown in Fig. 4.8 and Fig. 4.9 respectively. From Fig. 4.8 and Fig. 4.9 it is seen that the quantum mechanical inversion layer charge concentration increases considerably as the surface potential as well as gate voltage increase.

The inversion carrier concentration for three doping concentration as a function of gate voltage for channel doping $N_A=1.1 \times 10^{24} \text{ m}^{-3}$ is shown in Fig.4.10. From Fig. 4.10 it is seen that the requirement of gate voltage increases with the increase of channel doping to get a fixed amount of inversion carrier concentration. In the inversion mode of operation of MOS structure the depletion carrier concentration will not change with the further increase of gate voltage. But the depletion carrier concentration increases with the increase of channel doping. For a fixed gate voltage the summation of inversion and depletion charge is almost fixed. The depletion charge increases with the increase of channel doping. Therefore, the inversion charge decreases with the increase of channel doping for a fixed gate voltage.

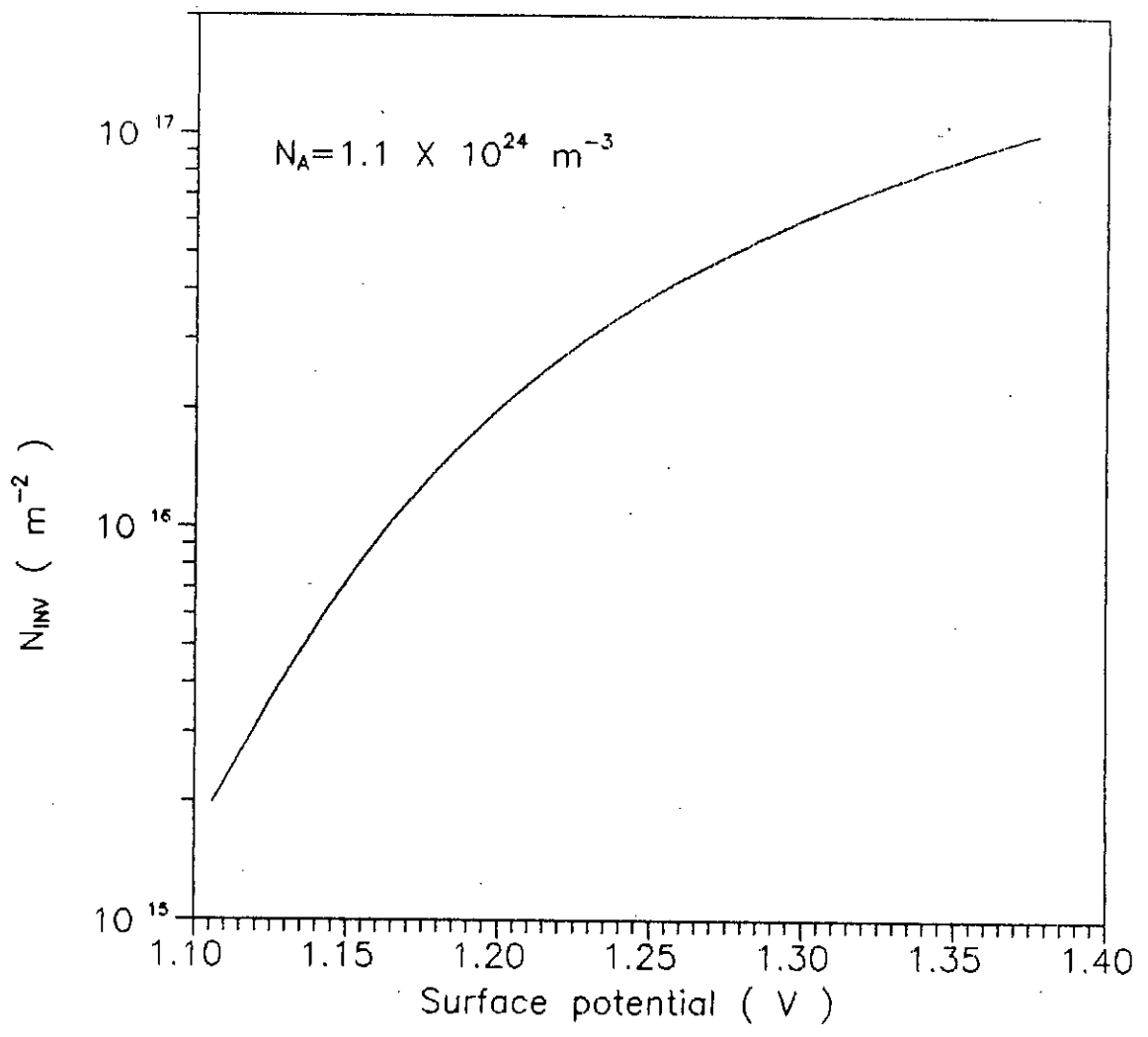


Fig. 4.8 Inversion layer carrier concentration vs. surface potential

89503

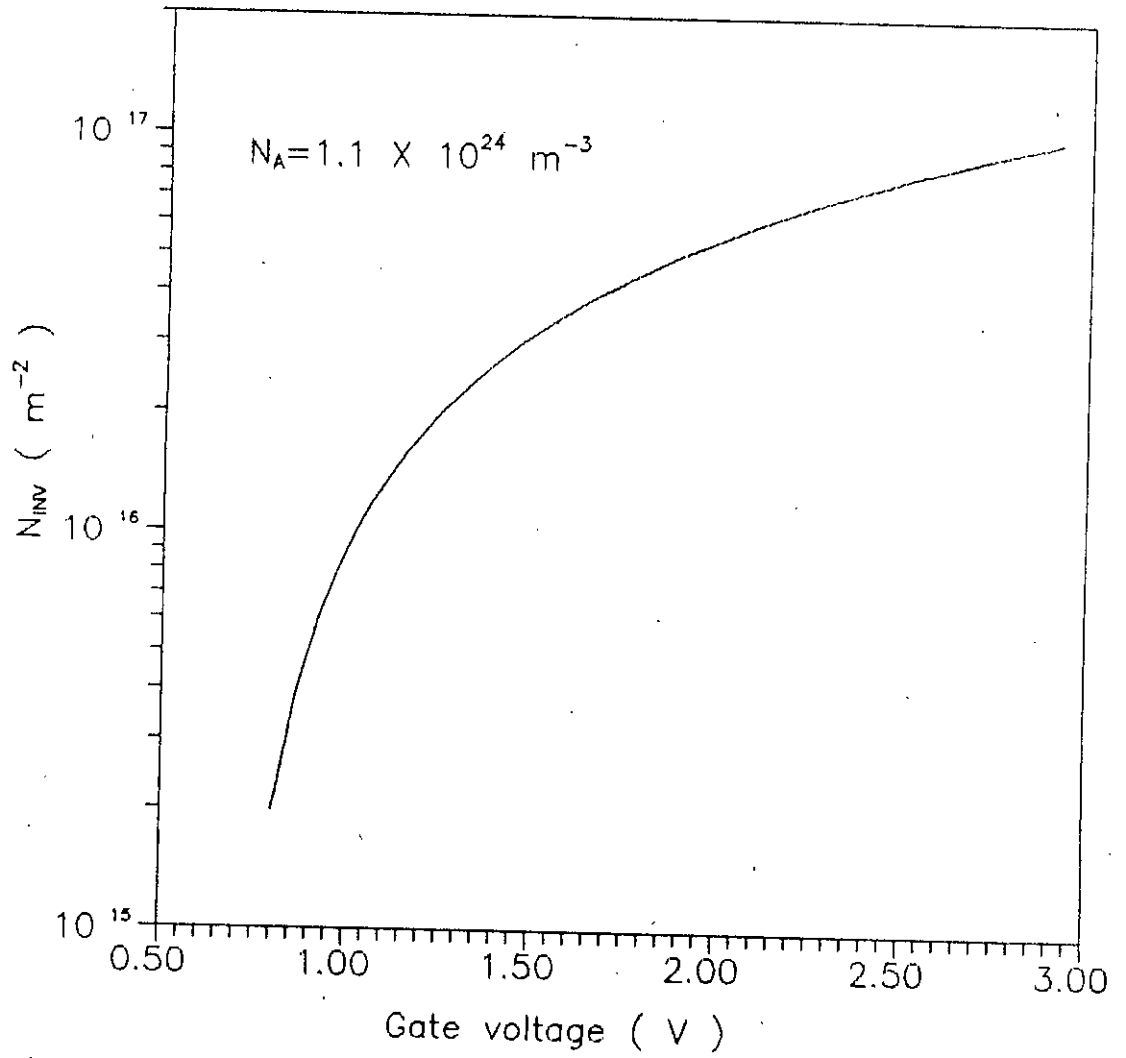


Fig. 4.9 Inversion layer carrier concentration vs. gate voltage

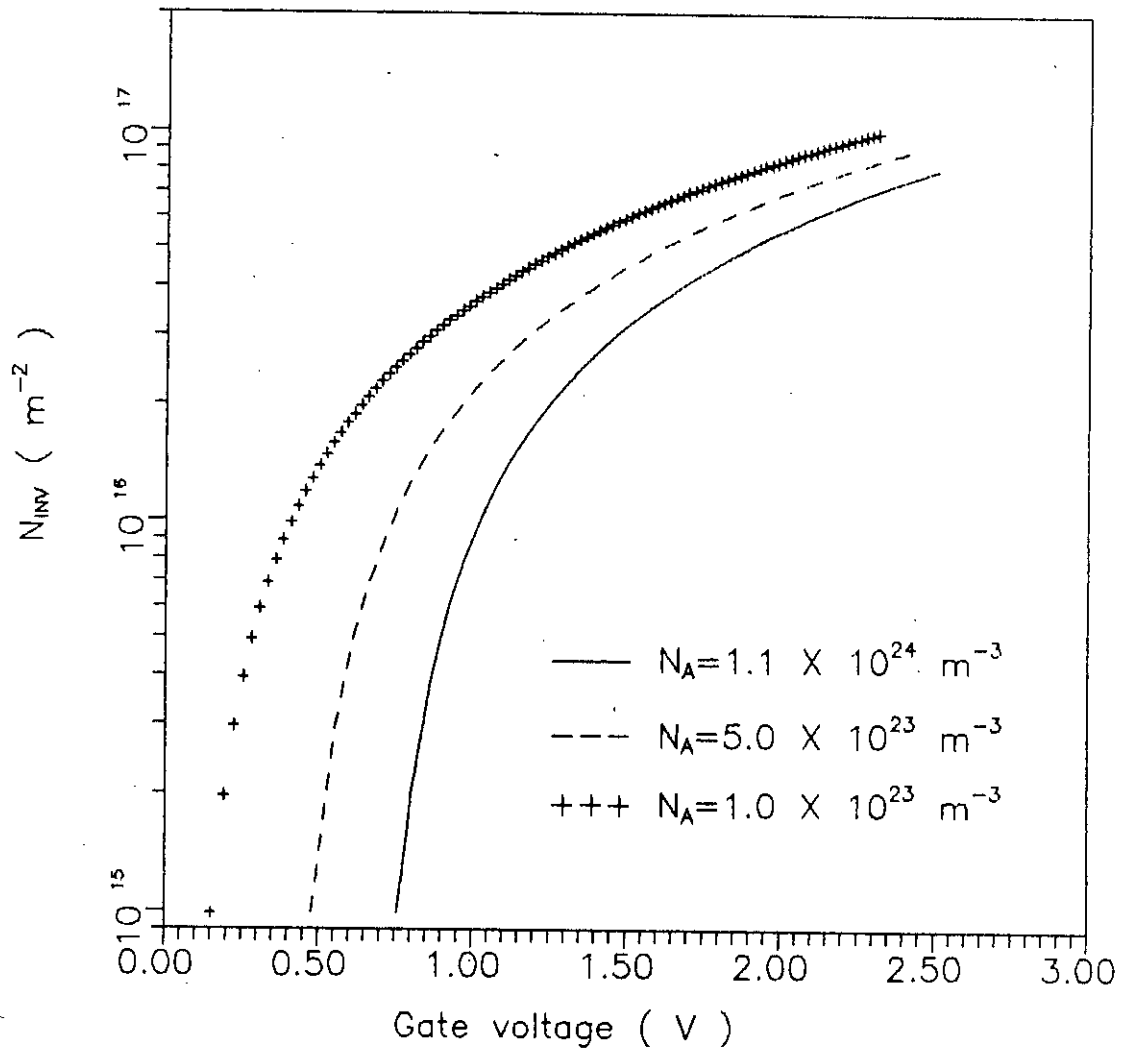


Fig. 4.10 Inversion layer carrier concentration vs. gate voltage for three different channel doping

4.3.1 Electron concentration in three subbands

The electron concentration in the three subbands as a function of surface potential is shown in Fig. 4.11 . Although energy levels $E_{20} \cong E_{11}$, the ground state of second valley (level 2,0) is favored by the electrons because of the larger density of states and higher valley degeneracy.

4.3.2 Depletion layer carrier concentration

The depletion layer carrier concentration as a function of surface potential with uniform channel doping is given in Fig. 4.12 . From Fig. 4.12 it is seen that the variation of depletion layer charge with the surface potential is very small compared to the inversion layer charge. After strong inversion, a small increase of ψ_s produces a large increase of electrons at the surface and the inversion layer acts like a narrow n^+ layer by shielding the semiconductor from further penetration of the electric field. Therefore the depletion layer charge remains constant and after strong inversion the depletion layer width becomes fixed.

4.3.3 Average spatial extent of the inversion layer electrons from the surface

The average potential of the inversion layer charge concentration from the surface Z_{av} as a function of the inversion layer charge concentration and the

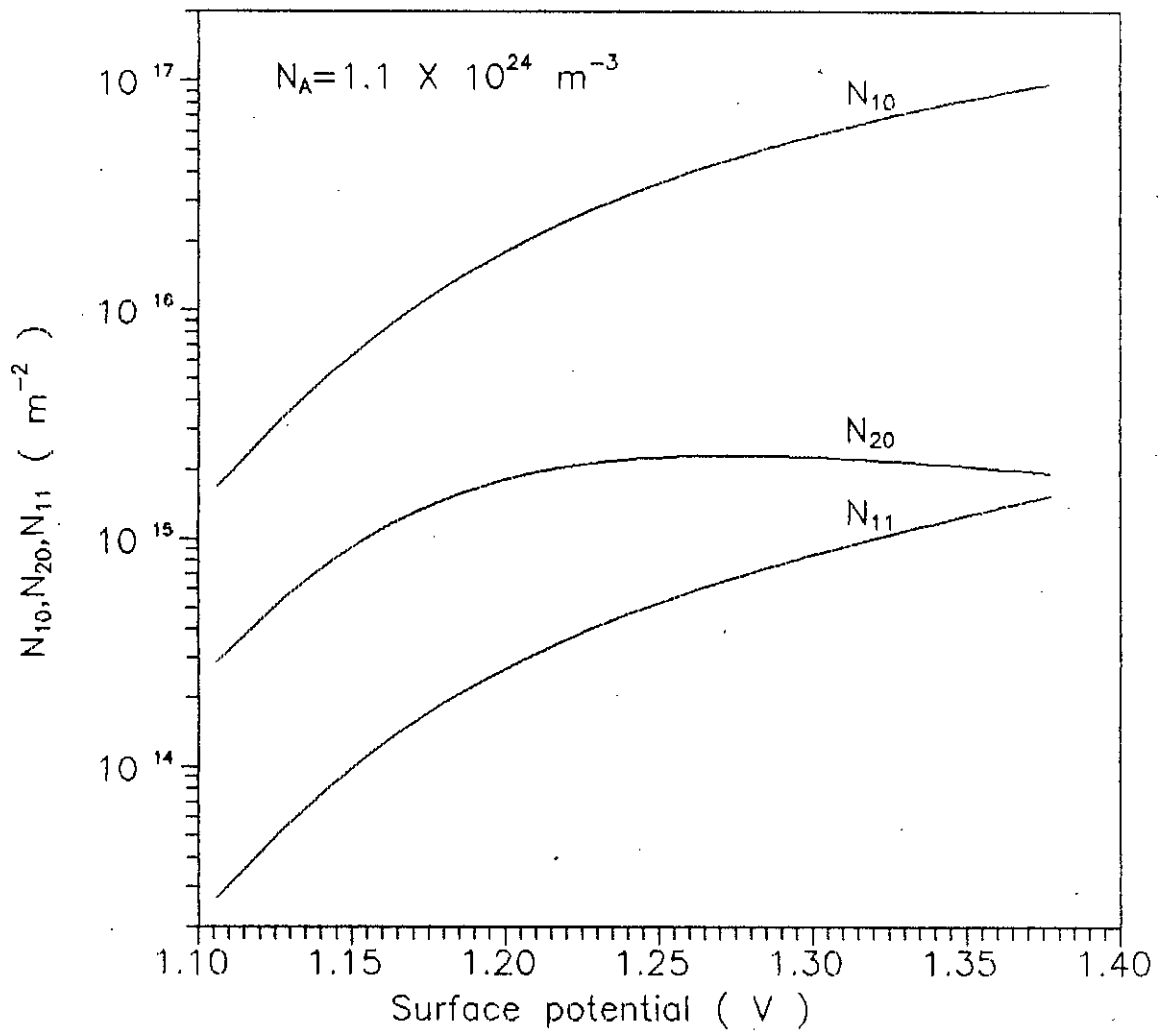


Fig. 4.11 Electron concentration in the three subbands vs. surface potential

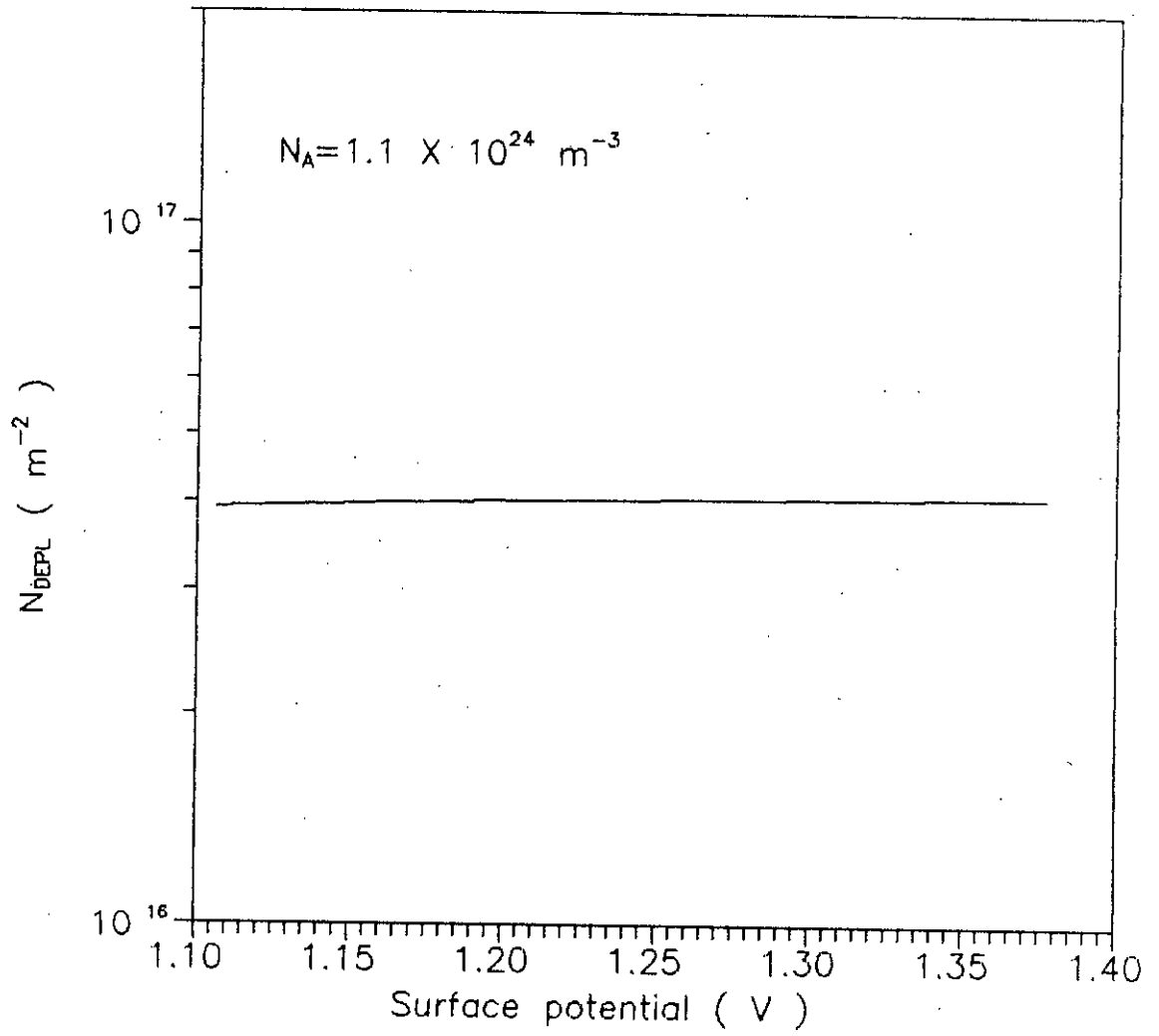


Fig. 4.12 Depletion carrier concentration vs. surface potential

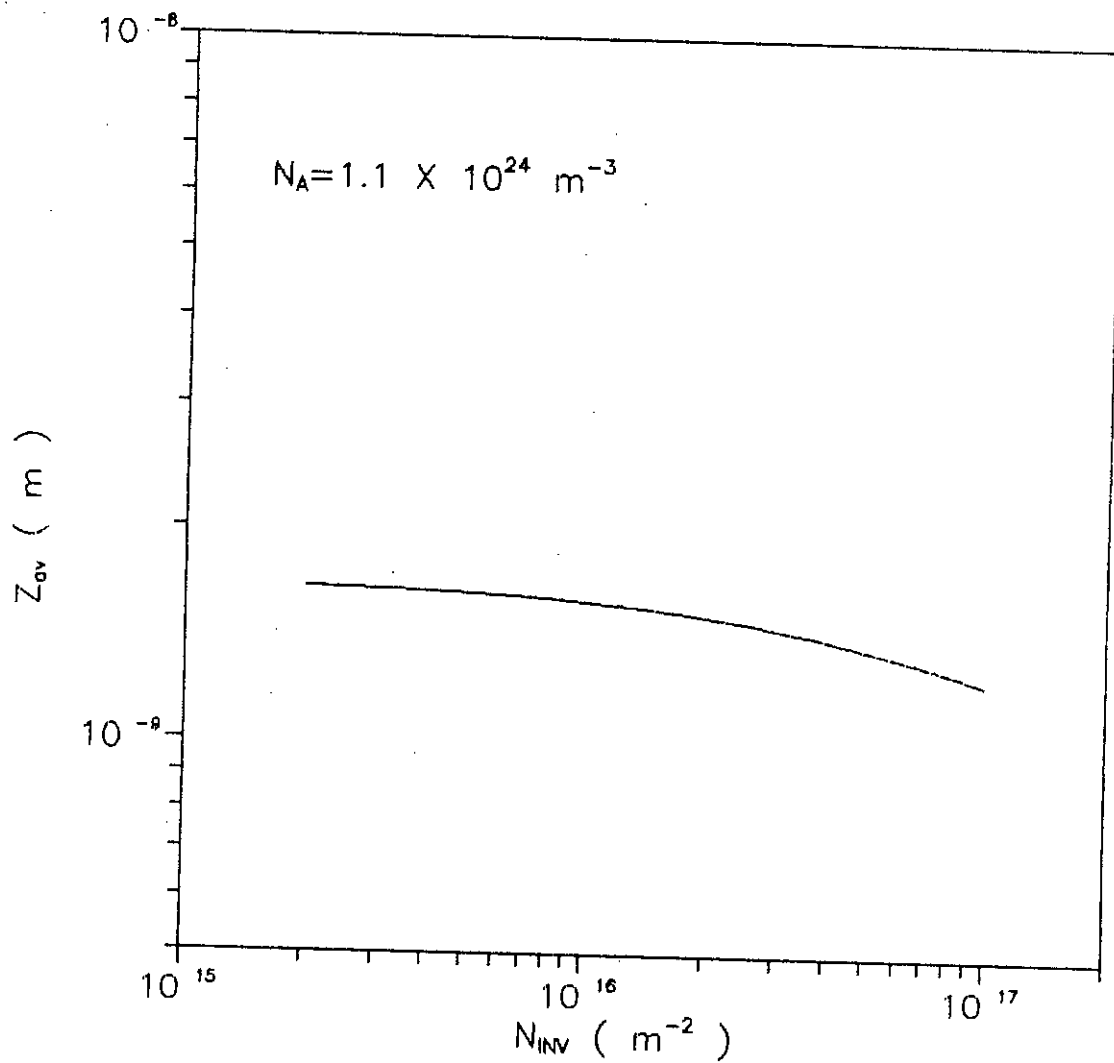


Fig. 4.13 Effect of inversion layer charge on average spatial extent of the inversion charges from the SiO_2 -Si interface

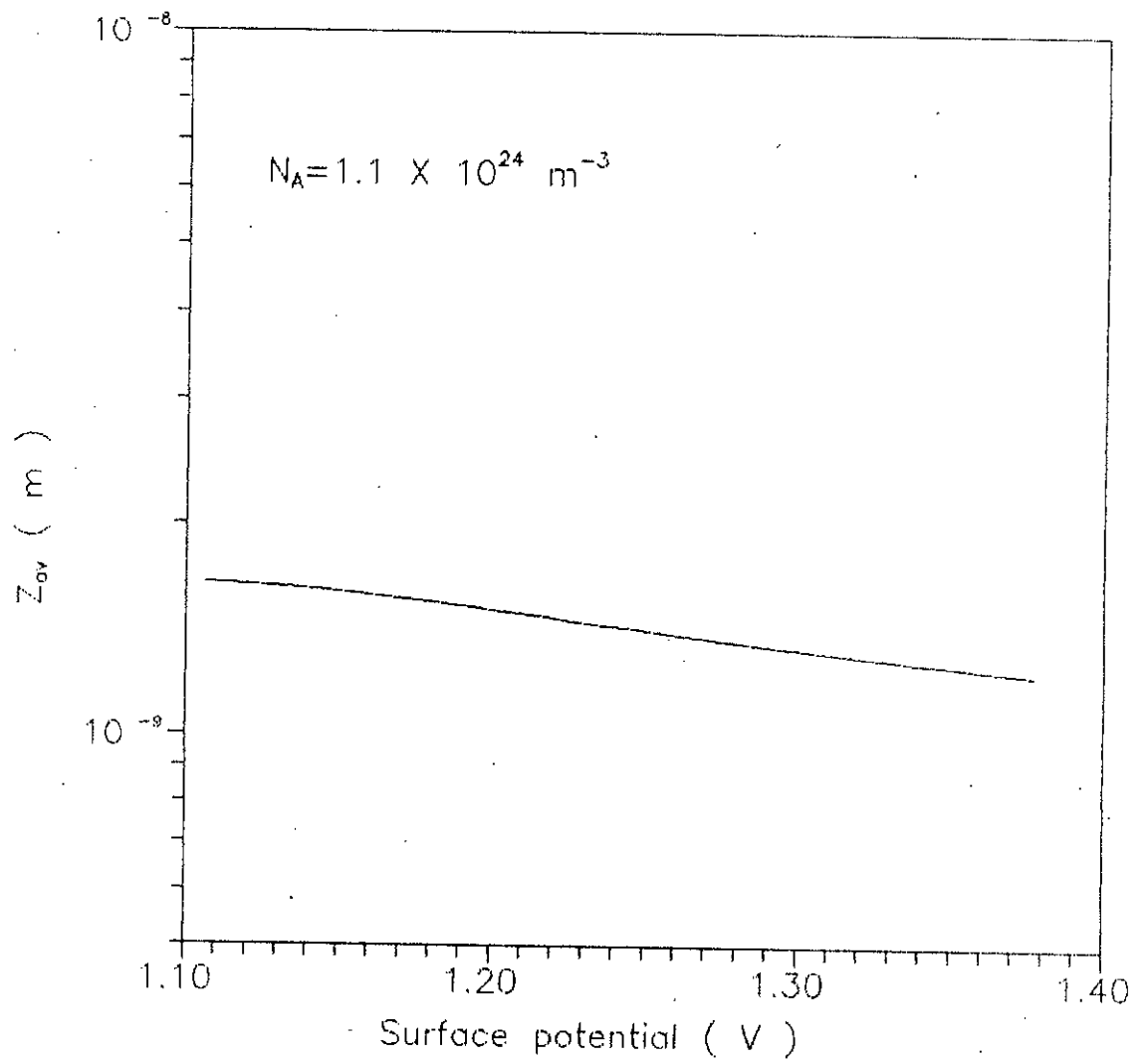


Fig. 4.14 Effect of surface potential on average spatial extent of the inversion charges from the SiO_2 -Si interface

surface potential with channel doping $1.1 \times 10^{24} \text{ m}^{-3}$ are shown in Fig. 4.13 and Fig. 4.14 respectively. The decrease of Z_{av} with increasing inversion layer charge is a reflection of the increasing surface electric field seen by the electrons which pushes them closer to the surface.

4.4 Inversion layer quantum capacitance

The inversion layer quantum capacitance as a function of surface potential and gate voltage for uniform channel doping of $5 \times 10^{23} \text{ m}^{-3}$ are shown in Fig. 4.15 and Fig. 4.16 . The predicted difference between quantum mechanically and classically calculated capacitance in inversion for an MOS capacitance with a uniform channel doping of $5 \times 10^{23} \text{ m}^{-3}$ are shown in Fig. 4.17 and Fig. 4.18 . It is seen from these figures that the difference between the quantum mechanically calculated capacitance and the classically calculated capacitance increases markedly with the increase of surface potential as well as gate voltage. The variation of inversion layer quantum capacitance with the applied surface potential is small compared to that calculated classically because with the increase of ψ_s both the energy levels (E_{10} , E_{20} and E_{11}) and also Fermi energy level with respect to the bottom of the conduction band at the silicon surface shifted upward and the number of inversion layer carriers cannot increase at the previous rate which is exponential in nature. But classically calculated inversion charge is truly an exponential function of surface potential. Therefore, for a given value of surface potential (or gate voltage) the inversion layer capacitance calculated quantum mechanically will be smaller than when calculated classically.

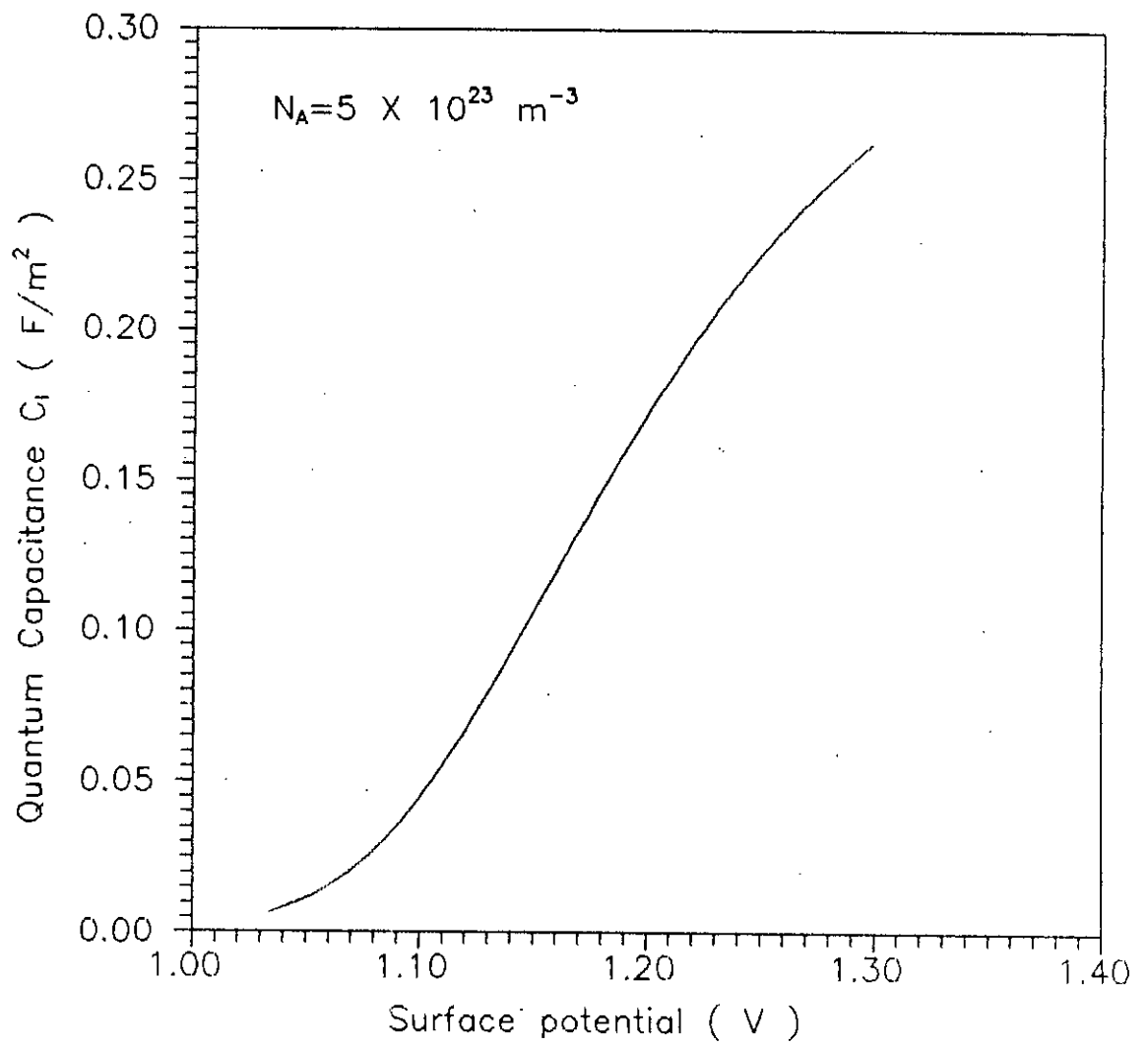


Fig. 4.15 Inversion layer quantum capacitance vs. surface potential

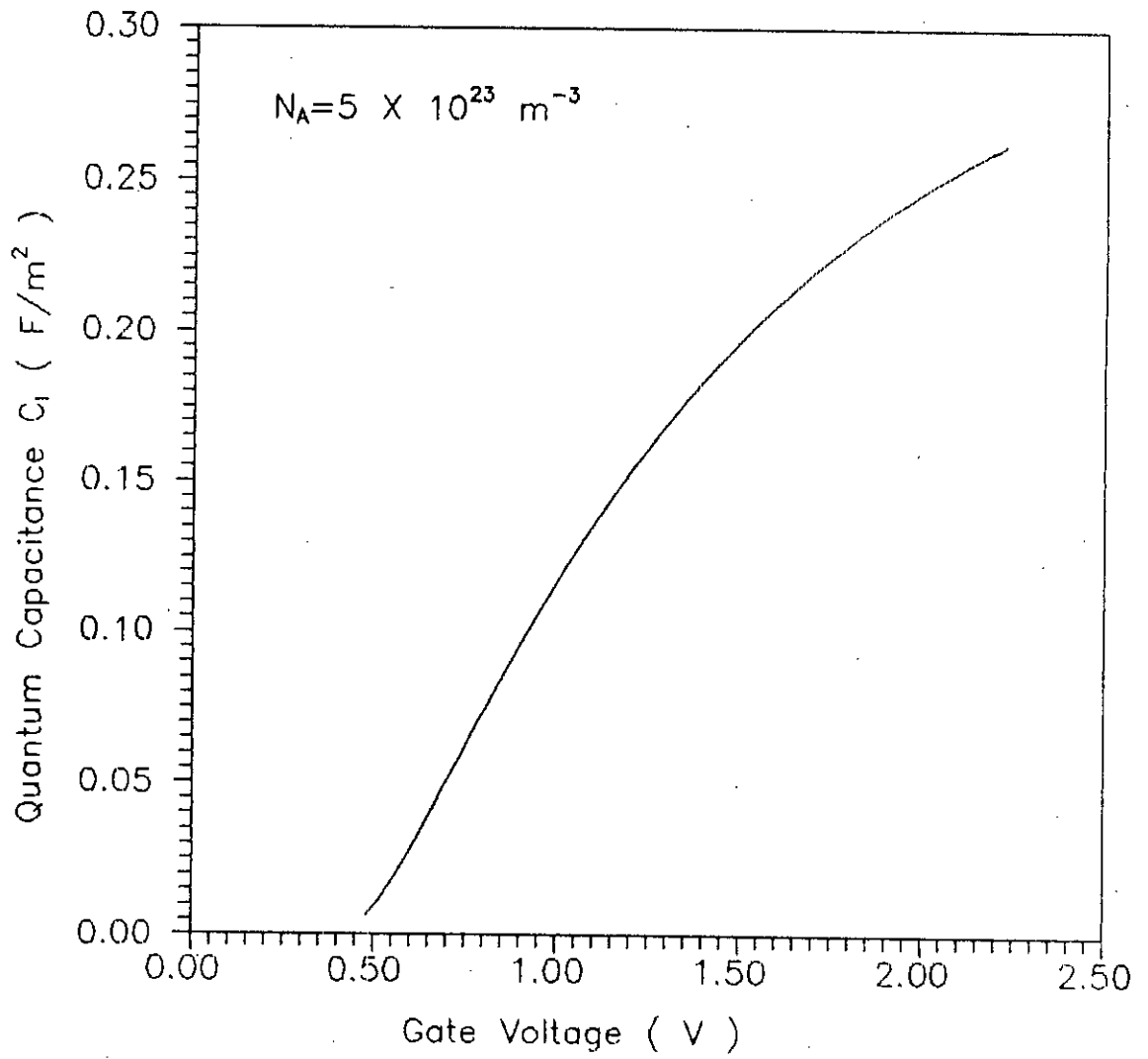


Fig. 4.16 Inversion layer quantum capacitance vs. gate voltage

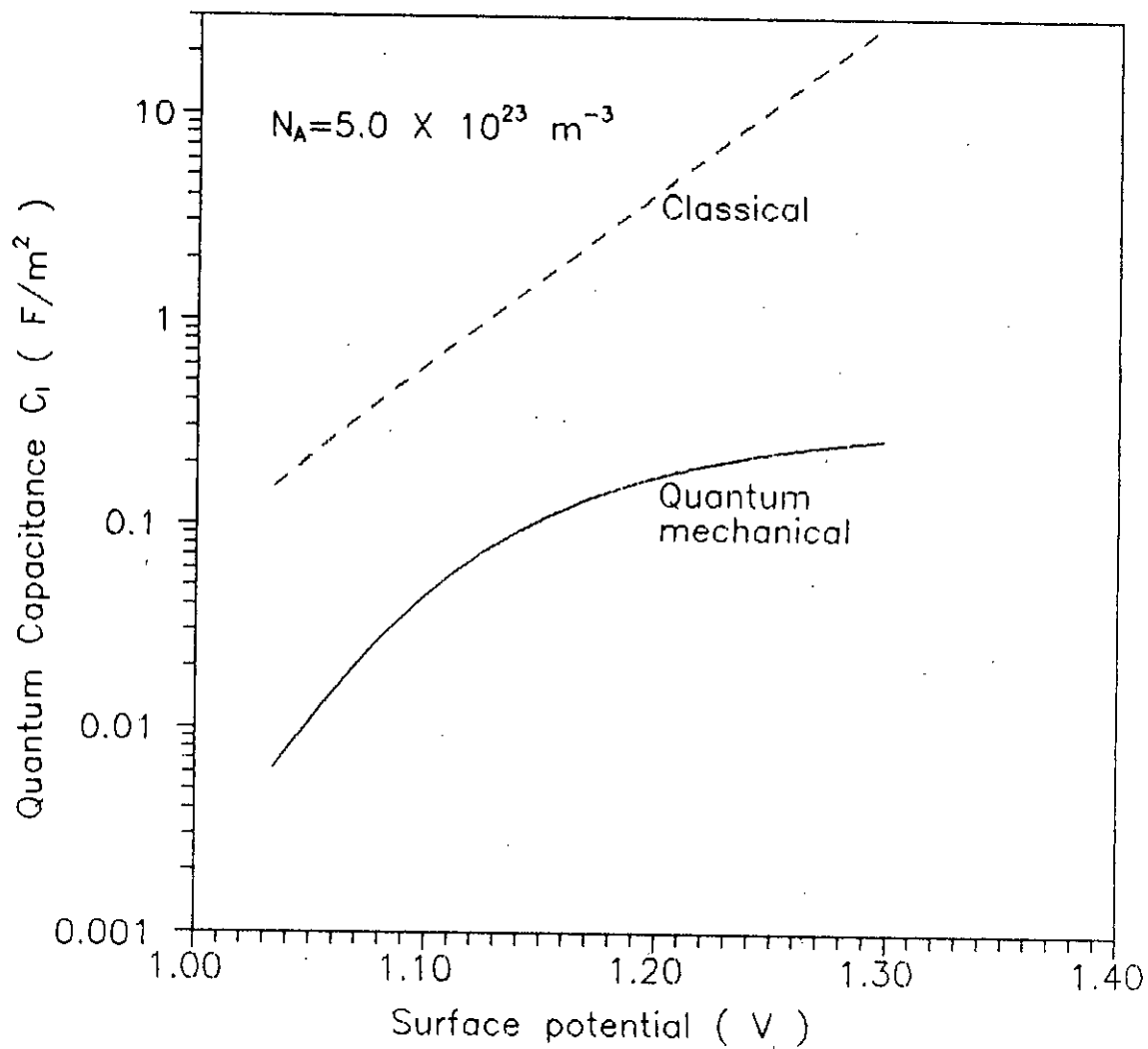


Fig. 4.17 Comparison of the effect of surface potential on inversion layer capacitance between classical and quantum mechanical calculations

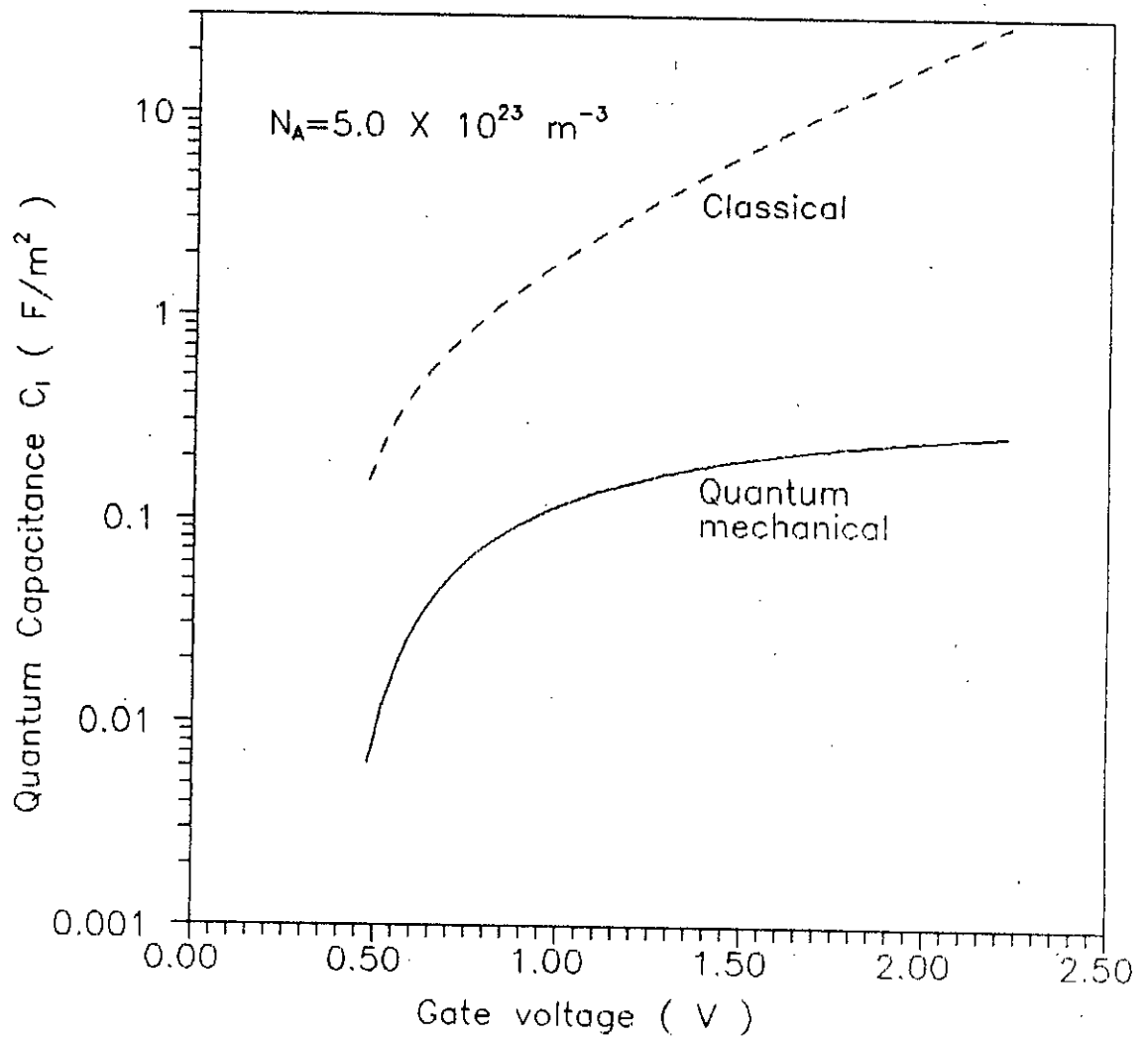


Fig. 4.18 Comparison of the effect of gate voltage on inversion layer capacitance between classical and quantum mechanical calculations

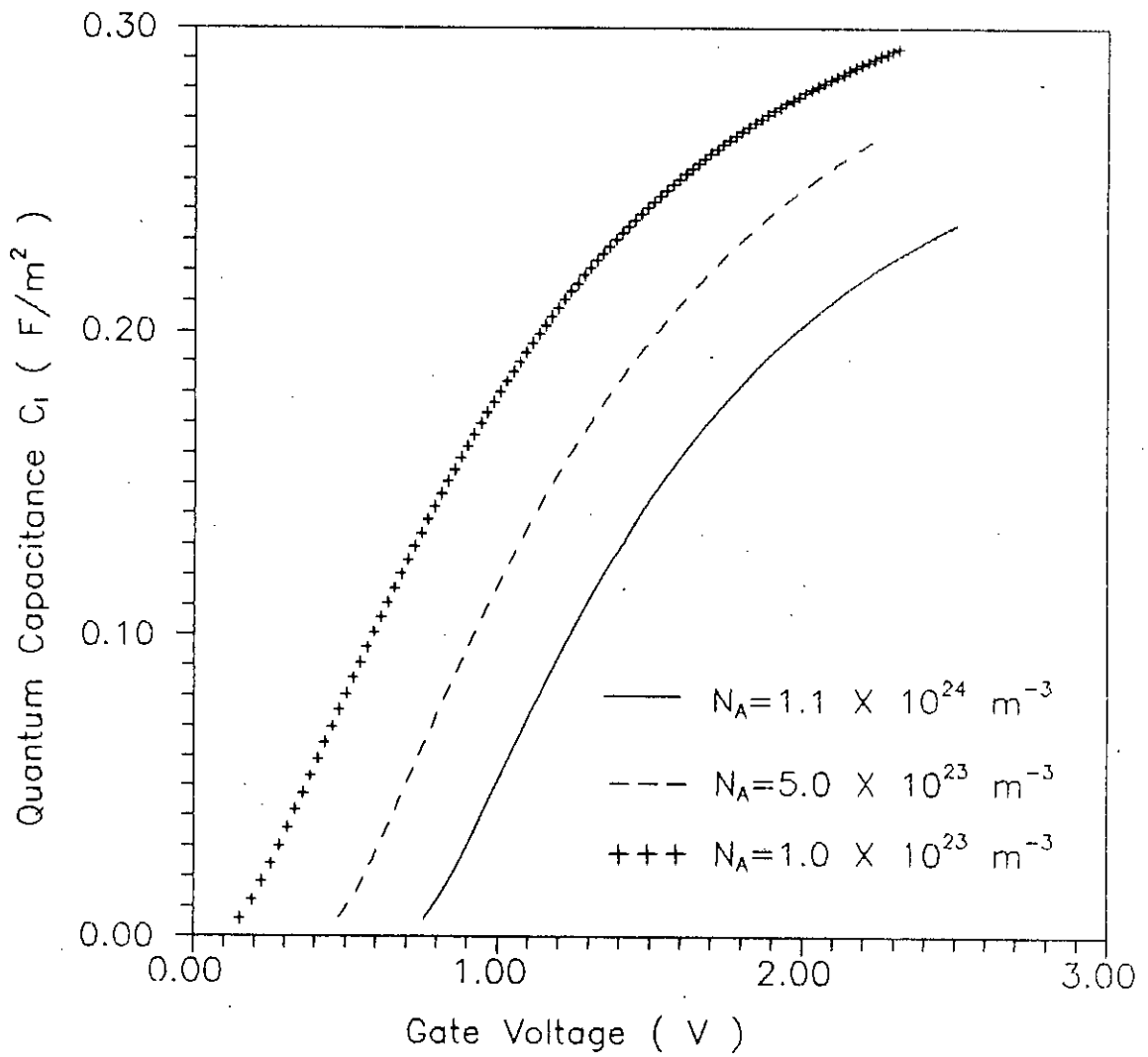


Fig. 4.19 Inversion layer quantum capacitance vs. gate voltage for three different channel doping

Fig. 4.19 shows the inversion layer quantum capacitance as a function of gate voltage for different channel doping. The channel doping levels are $1.1 \times 10^{24} \text{ m}^{-3}$, $5.0 \times 10^{23} \text{ m}^{-3}$ and $1.0 \times 10^{23} \text{ m}^{-3}$. For a fixed gate voltage, the inversion layer quantum capacitance decreases with the increase of channel doping because inversion layer carrier concentration decreases with the increase of channel doping for a fixed gate voltage (Fig. 4.9).

4.5 Total gate capacitance

The total gate capacitance calculated as a function of gate voltage both quantum mechanically (solid line) and classically (dashed line) for channel doping of $5 \times 10^{23} \text{ m}^{-3}$ is shown in Fig. 4.20 . The difference between the quantum mechanically and classically calculated gate capacitance is due to the difference of inversion layer capacitance between those two methods (Fig.4.18).

The gate capacitance considering quantum mechanical effects as a function of gate voltage for three different channel doping is shown in Fig.4.21 .

At low frequencies, the inversion layer quantum capacitance has significant contribution on total gate capacitance. After strong inversion, the inversion layer quantum capacitance is much larger than the depletion capacitance. So, total gate capacitance is essentially equal to the series combination of oxide capacitance and inversion layer quantum capacitance. As

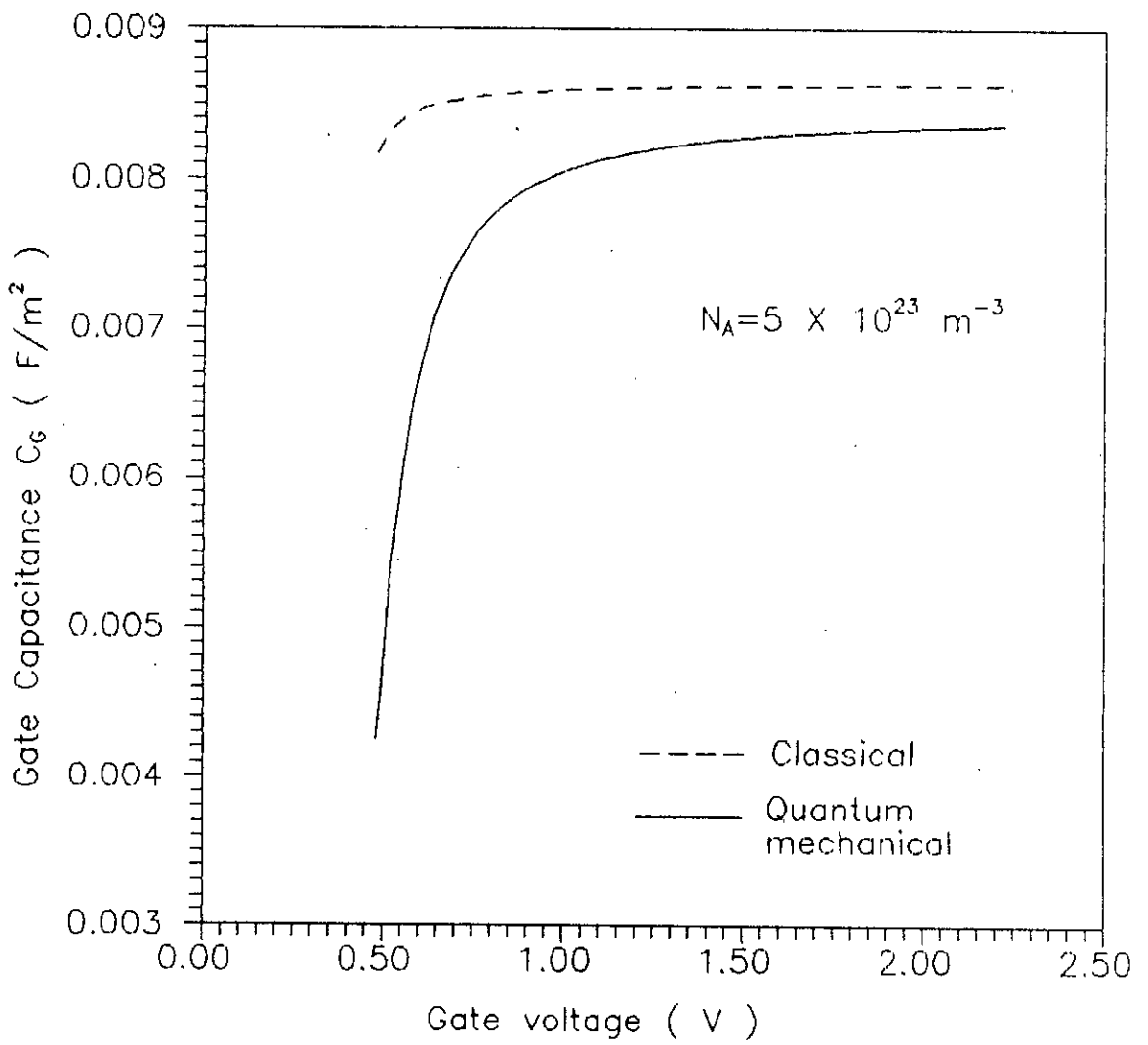


Fig. 4.20 Comparison of the effect of gate voltage on total gate capacitance between classical and quantum mechanical calculations

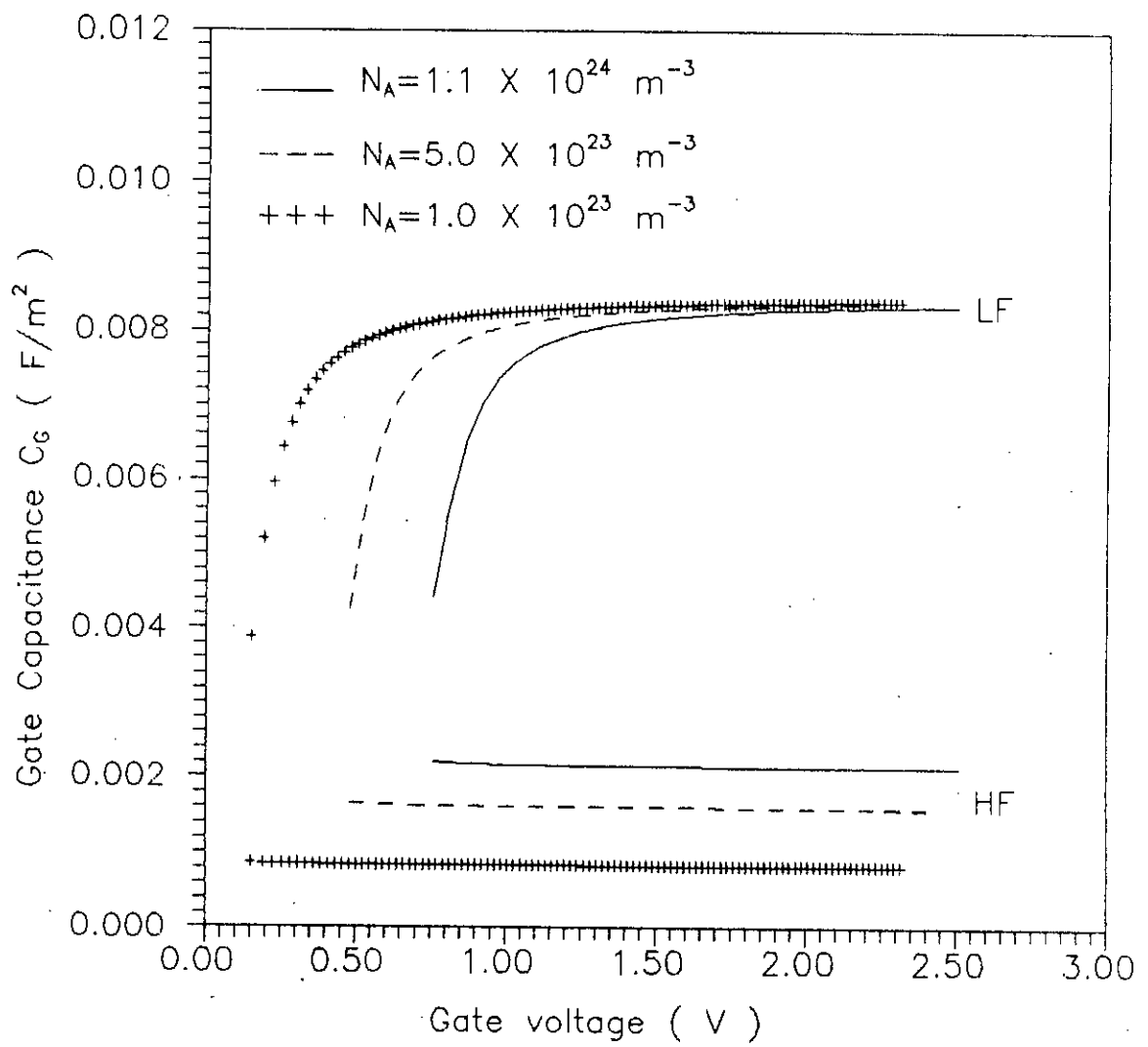


Fig. 4.21 High frequency and low frequency capacitance-voltage characteristics for three different channel doping

C_1 is much larger than C_0 , the total gate capacitance is approximately equal to the oxide capacitance when the device is more strongly inverted.

At high frequencies, it is seen from equation (3.37) that the inversion layer quantum capacitance has no contribution to the total gate capacitance. So, the total gate capacitance is essentially equal to the series combination of oxide capacitance (C_0) and depletion capacitance (C_D). As C_D is very small compared to C_0 , C_D dominates the total gate capacitance. With the increase of the channel doping, the maximum width of depletion layer decreases and the depletion capacitance increases. Thus, the total gate capacitance at high frequencies increases with the increase of channel doping as seen in Fig.21.

4.6 Conclusions

The analytical model developed in chapter two and chapter three is used here to study the quantum capacitance, frequency dependence of total gate capacitance and other characteristics of MOS device considering the quantum mechanical effects on the inversion layer minority carriers.

The first three consecutive subband energy levels with respect to the bottom of conduction band at SiO_2 -Si interface are studied and compared with self-consistent calculation results and found to closely agree with self-consistent results. Though the self-consistent calculation is accurate but it is very time consuming. But almost the same result is obtained by using variational

approximation method and it requires the same CPU time as that of the classical calculation.

The inversion layer carrier concentration for three different channel doping is studied and is seen that to get the same inversion layer carrier concentration the requirement of gate voltage increases with the increase of channel doping. The electron concentration in the three consecutive subbands is studied and is seen that relative occupation of carriers in the first subband increases with the increasing gate voltage.

The average separation of the inversion layer electrons from the $\text{SiO}_2\text{-Si}$ interface decreases with the increasing gate voltage.

The variation of inversion layer quantum capacitance and the total gate capacitance with the applied surface potential and gate voltage are studied and is found to be small compared to the classical one.

Finally, the frequency dependence of total gate capacitance for different channel doping is studied and is seen that the total gate capacitance decreases at high frequencies and increases at low frequencies.

CHAPTER 5

CONCLUSIONS

5.1 Conclusions

In this work, the total gate capacitance of submicron inversion MOS capacitor is studied. It is found that the total gate capacitance of MOS structure depends on gate voltage and frequency. Inversion layer quantum capacitance has significant contribution to the total gate capacitance. In order to calculate the inversion layer quantum capacitance, it is necessary to determine the subbands energy levels. In this work the analytical expressions of first three consecutive subband energy levels are determined using variational approximation method. It is very difficult to obtain the exact analytical expression for subband energy levels for arbitrary potential profile like that of MOS structure. However, the subband energy levels obtained by using variational approximation method is compared with that of the self-consistent results. It is found that our calculations of subband energy levels are in good agreement with the self-consistent results.

In equilibrium and at the relatively high transverse fields existing in submicron devices (even at zero gate drive), the lowest three energy levels are sufficient to account for most of inversion layer charge. This means that the occupancy of the energy levels higher than the third subband is sufficiently

negligible to be ignored without sacrificing accuracy. Very laborious work is required to determine the analytical expression for energy levels higher than third subband. In that case we should go for numerical solutions. The analytical expressions for subband energies of this work can be the basis of the numerical solution of the energy levels higher than the third subband.

5.2 Suggestions for future work

In order to determine the inversion layer quantum capacitance, the analytical expression of the first three subband energy levels are determined by using variational approximation method. The analytical expressions of these energy subbands can be used to calculate other parameters of MOS device considering quantum mechanical effects. The variational approximation method can be applied for an arbitrary potential profile to find analytical expression for energy subbands if the wave functions are assumed to have a predetermined form. So, this variational technique described in the calculation of subband energy levels in chapter two can be applied to other types of device for the calculation of the analytical expressions of subband energies.

REFERENCES

- [1] B. G. Streetman, "Solid State Electronic Devices," Prentice Hall, New York, 1990, pp. 301-308.
- [2] Sze, S. M. "Physics of Semiconductor Devices," 2nd edition, Wiley, New York, 1983, pp. 372-374.
- [3] Yannis P. Tsividis, "Operation and Modeling of the MOS Transistor," McGraw-Hill, New York, 1987, pp. 47-66.
- [4] Dieter K. Schroder, "Advanced MOS Devices," Modular series on solid state devices, Arizona State University, 1987, pp. 22-26.
- [5] C. Mogletue, "Self Consistent Calculation of Electron and Hole Inversion Charges at the Silicon-Silicon Dioxide Interfaces," *Journal of Applied Physics*, Vol. 59, No. 9, 1986, pp. 3175-3183.
- [6] F. Stern, "Self Consistent Results for n-Type Si Inversion Layers," *Physical Review B*, Vol. 5, No. 12, 1972, pp. 4891-4899.
- [7] Y. Ohkura, "Quantum Effects in Si n-MOS Inversion Layer at High Substrate Concentration," *Solid State Electronics*, Vol. 33, No. 12, 1990, pp. 1581-1585.

- [8] M. J. Van Dort et al. , "A Simple Model for Quantization Effects in Heavily-Doped Silicon MOSFET's at Inversion Conditions," *Solid State Electronics*, Vol. 37, No. 3, 1994, pp. 411-414.
- [9] Surge Luryi, "Quantum Capacitance Devices," *Applied physics letters*, Vol. 52(6), 1988, pp. 501-503.
- [10] Maherin Matin , "A study of Inversion Layer Quantum Capacitance of MOS Structures," *M.Sc. Engineering thesis*, BUET, Dhaka, Bangladesh.
- [11] S. Krishnamurthy et al. , "Modeling of Inversion Layer Quantization in Deep submicron N-channel MOS Devices," *Technical Report*, Department of Electrical and Computer Engineering, Microelectronics Research Center, The University of Texas at Austin, 1994.
- [12] Jan Genoe et al. , "Capacitance's in Double-Barrier Tunneling Structures," *IEEE Transactions On Electron Devices*, Vol. 38, No. 9, September, 1991, pp. 2006-2012.
- [13] W. Magnus, C. Sala and K. De Meyer, "Quantized Energy Levels in Si Inversion Layers; A simplified Self-Consistent Approach," *Journal of Applied Physics*, Vol. 63(8), 1988, pp. 2704-2710.

- [14] Baccarani and M.R. Wordeman, "Transconductance Degradation in Thin-Oxide MOSFET's , " *IEEE Transactions on Electron Devices*, Vol. ED-30, No. 10, 1983, pp. 1295-1304.
- [15] Leonard I. Schiff, " Quantum Mechanics," McGraw-Hill, New York, 1968, pp. 255-257.
- [16] S. R. Hofstein and G. Warfield, "Physical Limitations on the Frequency Response of a Semiconductor Surface Inversion Layers," *Solid State Electronics*, vol. 8, 1965, pp. 321-341.
- [17] K. Lehovec and A. Slobodskoy, "Impedance of Semiconductor-insulator-metal Capacitors," *Solid State Electronics*, vol. 7, 1964, pp. 59-79.
- [18] E.S. Yang , "Microelectronic Devices," McGraw-Hill Book company, New York, 1988 , pp. 428-430.

APPENDIX I

RESISTANCE ASSOCIATED WITH THE DIFFUSION CURRENT OF ELECTRONS FROM THE BULK TO THE EDGE OF THE DEPLETION REGION

The “driving force” for the excess-electron current, which results from in the region of quasi-neutrality $z \geq Z_d$, is not an ordinary potential, but the concentration potential, (i.e. potential due to concentration variation of electron at $z = Z_d$)

$$v_{n,d} = \frac{\tilde{n}_d}{n_0\beta} \quad ; \quad \beta = \frac{q}{kT} \quad (I-1)$$

Where n_0 is the electrons concentration in the bulk and \tilde{n}_d is the concentration variation of electron at $z = Z_d$.

The continuity equation for electrons can be written as,

$$\frac{\partial \delta_n}{\partial t} = -\frac{\delta_n}{\tau_n} + D_n \frac{\partial^2 \delta_n}{\partial z^2} \quad (I-2)$$

Where, τ_n is the minority carrier life-time and δ_n is the concentration of excess electron.

By solving the continuity equation (I-2), we get ,

$$j\omega \tilde{n} = -\frac{\tilde{n}}{\tau_n} + D_n \frac{\partial^2 \tilde{n}}{\partial z^2} \quad (I-3)$$

Where \tilde{n} concentration variation of electron .

Equation (I-3) can be written as

$$\tilde{n} \frac{(1 + j\omega\tau_n)}{D_n\tau_n} = \frac{\partial^2 \tilde{n}}{\partial z^2} \quad (I-4)$$

Solving equation (I-4) we get,

$$\tilde{n} = C_1 e^{-\left(\sqrt{\frac{(1+j\omega\tau_n)}{D_n\tau_n}}\right)z} + C_2 e^{\left(\sqrt{\frac{(1+j\omega\tau_n)}{D_n\tau_n}}\right)z} \quad (I-5)$$

Boundary conditions are, at $z = Z_d$, $\tilde{n} = \tilde{n}_d$ and at $z \rightarrow \infty$, $\tilde{n} = 0$

$$\tilde{n} = \tilde{n}_d e^{-\left(\sqrt{\frac{(1+j\omega\tau_n)}{D_n\tau_n}}\right)(z-Z_d)} \quad (I-6)$$

Diffusion current can be written as,

$$\begin{aligned} i_{n,d} &= qD_n \frac{d\tilde{n}(z)}{dz} \\ &= qD_n \tilde{n}_d e^{-\left(\sqrt{\frac{(1+j\omega\tau_n)}{D_n\tau_n}}\right)(z-Z_d)} \left\{ \sqrt{\frac{(1+j\omega\tau_n)}{D_n\tau_n}} \right\} \end{aligned} \quad (I-7)$$

At $z = Z_d$

$$i_{n,d} = qD_n \tilde{n}_d \left\{ \sqrt{\frac{(1+j\omega\tau_n)}{D_n\tau_n}} \right\} \quad (I-8)$$

$$\therefore \frac{i_{n,d} n_0 \beta}{\tilde{n}_d} = q\mu_n n_0 \left\{ \sqrt{\frac{(1+j\omega\tau_n)}{D_n\tau_n}} \right\} \quad (I-9)$$

Resistance is the ratio of voltage and current,

$$\therefore R_{n,B} = \frac{v_{n,d}}{i_{n,d}} = \frac{\tilde{n}_d}{n_0 \beta i_n} \quad (I-10)$$

From equation (I-9) we get,

$$\frac{1}{R_{n,B}} = q\mu_n n_0 \left\{ \sqrt{\frac{(1+j\omega\tau_n)}{D_n\tau_n}} \right\} \quad (I-11)$$

$$\therefore R_{n,B} = \frac{(D_n\tau_n)^{\frac{1}{2}}}{q\mu_n n_0 (1+j\omega\tau_n)^{\frac{1}{2}}} \quad (I-12)$$

For frequencies substantially below the inverse of the minority carrier lifetime, the bulk diffusion resistance is,

$$R_{n,B} = \frac{(D_n \tau_n)^{\frac{1}{2}}}{q \mu_n n_0} \quad (I-13)$$

APPENDIX II

EFFECTIVE RESISTANCE OF DEPLETION REGION TO FLOW OF MINORITY AND MAJORITY CARRIERS

We assume a p-type substrate with a uniform doping concentration N_A , and approximate the dependence of voltage with position as

$$V(z) = \frac{N_A q}{2\epsilon_s} z^2 \quad (\text{II-1})$$

$$\text{or, } \beta V(z) = \left(\frac{z}{\lambda_D} \right)^2 = y^2 \quad (\text{II-2})$$

$$\text{with } \lambda_D = \left[\frac{\epsilon_s}{q N_A \beta} \right]^{\frac{1}{2}}$$

Where λ_D is a Debye length based on the charge concentration qN_A . For simplicity we have assumed $z = 0$ at the bulk edge of the depletion layer and $z = d$ at the semiconductor-insulator interface.

The resistance $R_{n,D}$ associated with the flow of minority carriers through the depletion layer is given by

$$R_{n,D} = \int_0^d \frac{dz}{\sigma_n(z)} = \int_0^d \frac{dz}{q\mu_n n(z)} = \frac{1}{q\mu_n n_1^2} \int_0^d p(z) dz \quad (\text{II-3})$$

Using the relation,

$$p(z) = N_A e^{-\beta V} \quad (\text{II-4})$$

We can write equation (II-3) as ,

$$R_{n,D} = \frac{N_A \lambda_D}{q \mu_n n_i^2} \int_0^{\frac{d}{\lambda_D}} e^{-y^2} dz \quad (\text{II-5})$$

Since typically $\frac{d}{\lambda_D} \gg 1$, we may take the upper limit as infinite so that the

magnitude of the integral is $\left(\frac{\pi}{2}\right)^{\frac{1}{2}} \approx 1$. Therefore

$$R_{n,D} \approx \frac{(\lambda_D N_A)}{\mu_n q n_i^2} = \frac{\lambda_D}{\mu_n q n_0} \quad (\text{II-6})$$

$$\text{Thus, } \frac{R_{n,B}}{R_{n,D}} = \frac{(D_n \tau_n)^{\frac{1}{2}}}{\lambda_D} = \frac{L_n}{\lambda_D} \quad (\text{II-7})$$

The magnitudes of these parameters for typical silicon structures are $L_n \approx 5 \times 10^{-5}$ meter, $\lambda_D \approx 1.3 \times 10^{-8}$ meter for $N_A = 10^{23} / \text{m}^3$. Therefore,

$$\frac{R_{n,B}}{R_{n,D}} \approx 3 \times 10^3 \quad (\text{II-8})$$

So, we can neglect $R_{n,D}$ in comparison with $R_{n,B}$.

APPENDIX III

RESISTANCE ASSOCIATED WITH THE GENERATION CURRENT WITHIN THE DEPLETION REGION

The recombination and generation of electrons and holes in semiconductors may take place at some type of recombination-generation centers or traps. These sites may be crystal lattice dislocations, impurity atoms located interstitially or substitutionally in the crystal lattice, or surface defects. The net recombination rate can be given as [18],

$$U = \frac{CN_t(pn - n_i^2)}{n + p + 2n_i \cosh\left[\frac{(E_t - E_i)}{kT}\right]} \quad \text{nos/ sec} \quad (\text{III-1})$$

Where, C is the capture coefficient, N_t is the density of centers, E_t is the energy of the centers, and E_i is the center of the forbidden energy gap.

For the special case of single set of traps at the center of the forbidden gap (i.e. $E_t = E_i$),

$$\text{So, } U = \frac{CN_t(pn - n_i^2)}{n + p + 2n_i} \quad (\text{III-2})$$

After applying gate voltage, the holes are rapidly swept out of depletion region by the large electric field, thus its density are small compared to n_i . For this case, recombination rate,

$$U = -\frac{CN_t n_i}{2} \quad (\text{III-3})$$

A negative recombination rate means a positive generation rate, and the resulting current is a generation current instead of a recombination current. So, the generation current,

$$I_G = qA|U|Z_d$$

$$I_G = \frac{qAn_iZ_dCN_t}{2} \quad (\text{III-4})$$

Where, Z_d is the depletion layer width, A is the area of the MOS structure. The minority carrier life-time can be written as

$$\tau_0 = \frac{1}{CN_t} \quad (\text{III-5})$$

So, the equation (III-4) becomes,

$$I_G = \frac{qAn_iZ_d}{2\tau_0} \quad (\text{III-6})$$

Resistance associated with this generation current,

$$R_{gd} = \frac{\phi_d}{I_G} = \frac{2\tau_0\phi_d}{qn_iZ_d} \quad (\text{III-7})$$

